



OPTIMAL HYDRODYNAMIC DESIGN OF A TUBULAR PHOTOBIOREACTOR

MISS PINYAPORN WONGLUANG

A SPECIAL RESEARCH PROJECT SUBMITTED IN PARTIAL FULFILLMENT  
OF THE REQUIREMENTS FOR  
THE DEGREE OF MASTER OF ENGINEERING (CHEMICAL ENGINEERING)  
FACULTY OF ENGINEERING  
KING MONGKUT'S UNIVERSITY OF TECHNOLOGY THONBURI  
2011

Optimal Hydrodynamic Design of a Tubular Photobioreactor

Miss Pinyaporn Wongluang B.Eng. (Chemical Engineering)

A Special Research Project Submitted in Partial Fulfillment of the Requirements for  
The Degree of Master of Engineering (Chemical Engineering)

Faculty of Engineering

King Mongkut's University of Technology Thonburi

2011

Special Research Project Committee

..... (Asst. Prof. Asawin Meechai, Ph.D.)	Chairman of Special Research Project Committee
..... (Assoc. Prof. Thongchai Srinophakun, Ph.D.)	Member and Special Research Project Advisor
..... (Asst. Prof. Jindarat Pimsamarn, Ph.D.)	Member of Special Research Project Committee

Copyright reserved

Special Research Project Title	Optimal Hydrodynamic Design of a Tubular Photobioreactor
Special Research Project Credits	6
Candidate	Miss Pinyaporn Wongluang
Special Research Project Advisor	Assoc. Prof. Dr. Thongchai Srinophakun
Program	Master of Engineering
Field of Study	Chemical Engineering
Department	Chemical Engineering
Faculty	Engineering
B.E.	2554

### Abstract

Many types of photobioreactor have been designed for microalgae cultivation. This thesis focuses on the tubular photobioreactor which is a potential large-scale microalgae and a suitable type for outdoor mass culture. However, the deficiencies of this reactor are the dead zones around the bend and the pressure loss through the bend. Therefore, the designing of the optimal U-bend and 90 degree bend configurations in order to reduce the dead zone and the pressure loss are the main study. The geometry of the tubular photobioreactor was drawn and meshed by ICEM CFD program. Then, FLUENT software was used to simulate the flow behavior inside the tubular photobioreactor. The simulation result of the basic tubular photobioreactor shows the dead zone occurring around U-bend and 90 degree bend. Hence, new configurations of bends are proposed. There are 6 configurations of U-bend and 4 configurations of 90 degree bend. The result shows that the optimal configuration of U-bend has a the radius of curvature 0.35 m and the angle of arc 210 degree and the optimal configuration of 90 degree bend has a radius of curvature 0.3 m. The proposed U-bend can reduce the dead zone from the standard U-bend 9.459% and the pressure loss 12.534%, while the proposed 90 degree bend can reduce the dead zone by 21.618% and the pressure loss by 11.863%. In addition, the relationship between the air inlet velocity and the seawater velocity is illustrated in order to find the optimal air inlet velocity. The result shows that the optimal air inlet velocity of the basic tubular photobioreactor model is 0.072 m/s and the optimal air inlet velocity of the optimal tubular photobioreactor model is 0.061 m/s. Therefore, the proposed tubular photobioreactor can reduce the energy input due to aeration by 15.04%.

Keywords : Tubular photobioreactor design/ Algae cultivation / CFD

หัวข้อโครงการศึกษาวิจัย	การออกแบบเครื่องปฏิกรณ์ชีวภาพแบบท่อรับแสงที่เหมาะสมต่อการเคลื่อนที่ของของไหล
หน่วยกิต	6
ผู้เขียน	นางสาวกัญญพร วงศ์เหลือง
อาจารย์ที่ปรึกษา	รศ. ดร. ชงไชย ศรีนพคุณ
หลักสูตร	วิศวกรรมศาสตรมหาบัณฑิต
สาขาวิชา	วิศวกรรมเคมี
ภาควิชา	วิศวกรรมเคมี
คณะ	วิศวกรรมศาสตร์
พ.ศ.	2554

#### บทคัดย่อ

เครื่องปฏิกรณ์ชีวภาพที่ออกแบบสำหรับการเลี้ยงสาหร่ายมีหลายประเภท ในงานวิจัยนี้สนใจเครื่องปฏิกรณ์ชีวภาพแบบท่อรับแสง ซึ่งมีศักยภาพในการเลี้ยงสาหร่ายปริมาณมากและเหมาะสำหรับการเลี้ยงภายนอกอาคาร แต่อย่างไรก็ตามเครื่องปฏิกรณ์ประเภทนี้มีข้อบกพร่องคือ มีบริเวณที่ของไหลมีความเร็วต่ำเกินไปเกิดขึ้นที่ท่อโค้ง และเกิดการสูญเสียความดันผ่านท่อโค้งมาก ดังนั้นการออกแบบท่อโค้ง 90 องศา และท่อโค้งยู ของเครื่องปฏิกรณ์ชีวภาพแบบท่อรับแสง เพื่อที่จะลดบริเวณที่ของไหลมีความเร็วต่ำและการสูญเสียความดันผ่านท่อโค้ง ขณะที่ของไหลยังคงต้องมีสถานะการไหลแบบปั่นป่วนเพื่อป้องกันการตกตะกอนของสาหร่าย จึงถูกศึกษา เครื่องปฏิกรณ์ชีวภาพแบบท่อรับแสงถูกวาดและแบ่งปริมาตรเป็นขนาดเล็กๆ โดยโปรแกรม ICEM หลังจากนั้นโปรแกรม FLUENT จะถูกใช้ในจำลองพฤติกรรมการไหลภายในเครื่องปฏิกรณ์แบบท่อรับแสง โดยผลการจำลองเครื่องปฏิกรณ์แบบท่อรับแสง แสดงให้เห็นว่า มีบริเวณที่ของไหลมีความเร็วต่ำเกิดขึ้นบริเวณท่อโค้งที่อยู่ และท่อโค้ง 90 องศา ดังนั้นท่อโค้งแบบใหม่จึงถูกเสนอ โดยมีท่อโค้งตัวยู 6 แบบ และท่อโค้ง 90 องศา 4 แบบ ผลจากโปรแกรมแสดงให้เห็นว่า ท่อโค้งตัวยู ที่ดีที่สุด มีรัศมีความโค้ง 0.35 เมตร และ มุมของส่วนโค้ง 210 องศา ส่วนท่อโค้ง 90 องศา ที่ดีที่สุดมีรัศมีความโค้ง 0.3 เมตร ท่อโค้งตัวยู ที่ถูกเสนอสามารถลดบริเวณที่มีความเร็วต่ำลงจากท่อโค้งตัวยูแบบมาตรฐานได้ 9.459เปอร์เซ็นต์ และลดความดันสูญเสียได้ 12.534 เปอร์เซ็นต์ ท่อโค้ง 90 องศาที่ถูกเสนอ สามารถลดบริเวณที่มีความเร็วต่ำลงได้ 21.618 เปอร์เซ็นต์ และลดความดันสูญเสียได้ 11.863 เปอร์เซ็นต์ นอกจากนี้ความสัมพันธ์ระหว่างความเร็วขาเข้าของอากาศกับความเร็วน้ำทะเลถูกแสดง เพื่อหาค่าความเร็วอากาศขาเข้าที่เหมาะสมซึ่งผลแสดงให้เห็นว่า ความเร็วอากาศขาเข้าที่เหมาะสมของเครื่องปฏิกรณ์แบบท่อรับแสงมาตรฐานคือ 0.072 เมตรต่อวินาที และความเร็วอากาศขาเข้าที่เหมาะสมของเครื่องปฏิกรณ์แบบท่อรับแสงแบบ

ที่ดีที่สุด คือ 0.061 เมตรต่อวินาที ดังนั้นเครื่องปฏิกรณ์ชีวภาพแบบท่อรับแสงที่ดีที่สุด จึงสามารถลดการใช้พลังงานเนื่องมาจากการป้อนอากาศลงได้ 15.04%

คำสำคัญ : การออกแบบเครื่องปฏิกรณ์แบบท่อรับแสง / การเลี้ยงสาหร่าย / การคำนวณทางพลศาสตร์ของไหล

## **ACKNOWLEDGEMENTS**

This project could not have been perfectly completed without direct and indirect assistance from many people. Foremost, the author would like to express her gratitude to the advisor of this project, Assoc. Prof. Thongchai Srinophakun for all technical support and valuable guidance. Also, the author would like to particularly express special thanks to the supervisor, Prof. Yusuf Chisti of Massey University for the suggestion about this project and his kind support during the overseas study. In addition, the author would like to thank Asst. Prof. Asawin Meechai and Asst. Prof. Jindarat Pimsamarn, project committee members, for their attention to this research project and their valuable ideas to improve the work.

Moreover, the author would like to thank friends who gave many helpful suggestions and the staff of Chemical Engineering Practice School (ChEPS), Mrs. Chadaporn, who helped the author with communication and any important information used to finish the Master's degree. Lastly, the author would like to thank her family for their encouragement and all support.

# CONTENTS

	<b>PAGE</b>
ENGLISH ABSTRACT	i
THAI ABSTRACT	ii
ACKNOWLEDGEMENTS	iv
CONTENTS	v
LIST OF TABLES	vii
LIST OF FIGURES	viii
NOMENCLATURES	
 <b>CHAPTER</b>	
<b>1. INTRODUCTION</b>	<b>1</b>
1.1 Background	1
1.2 Objective	1
1.3 Scope of work	1
 <b>2. THEORY AND LITERATURE REVIEWS</b>	 <b>2</b>
2.1 Algae	2
2.2 Algae cultivation systems	4
2.2.1 Open systems	4
2.2.2 Closed systems	5
2.2.2.1 Flat-plate photobioreactor	5
2.2.2.2 Bubble column photobioreactor	6
2.2.2.3 Tubular photobioreactor	6
2.3. Criteria of the tubular photobioreactor design	7
2.4 Mechanical Energy Balance	8
2.5 Computational fluid dynamics (CFD)	11
2.5.1 Flow modeling	11
2.5.1.1 Turbulent modeling	11
2.5.1.2 Species modeling	11
 <b>3. METHODOLOGY</b>	 <b>12</b>
 <b>4. RESULTS AND DISCUSSION</b>	 <b>14</b>
4.1 Base model of the tubular photobioreactor	14
4.1.1 Effect of air velocity on the seawater velocity	14
4.1.2 Velocity profile of base model	15
4.1.3 Pressure loss of bends	17
4.2 Modified model of the tubular photobioreactor	19
4.2.1 U-bend configuration improvement	19
4.2.1.1 Seawater velocity analysis	19
4.2.1.2 Pressure loss comparisons	23

4.2.2 90 degree bend configuration improvement	24
4.2.2.1 Seawater velocity analysis	24
4.2.2.2 Pressure loss comparison	27
4.3 Optimal model of the tubular photobioreactor	28
<b>5. CONCLUSION AND RECOMMENDATION</b>	<b>30</b>
5.1 Conclusion	30
5.2 Recommendation	30
<b>REFERENCES</b>	<b>31</b>
<b>APPENDIX</b>	<b>33</b>
A. Tubular photobioreactor configuration	33
B. Histogram of dead zone	38
C. Pressure loss calculation	44
D. Program set up	47
<b>CURRICULUM VITAE</b>	<b>55</b>

**LIST OF TABLES**

<b>TABLE</b>	<b>PAGE</b>
4.1 Percentage of dead zone	23
4.2 Pressure loss of each U-bend and percentage of pressure loss reduction	23
4.3 Percentage of dead zone of 90 degree bend	27
4.4 Pressure loss of each 90 degree bend and percentage of pressure loss reduction	27
C.1 Pressure loss calculation of U-bend	45
C.2 Pressure loss calculation of 90 degree bend	45

## LIST OF FIGURES

FIGURE	PAGE
2.1 Cyanobacteria (blue – green algae)	2
2.2 Phaeophyta (brown-kelps) and Rhodophyta (red)	3
2.3 Coccoid algae	3
2.4 Aerial schematic view of a raceway pond	4
2.5 Flat-plate photobioreactor	5
2.6 Bubble column photobioreactor	6
2.7 Tubular photobioreactor	7
2.8 Tubular photobioreactor with details of the solar loop (a) and the degasser zone (b)	7
2.9 The position of fluid flow at $t \geq 0$	8
2.10 The control volume of fluid flow system	9
3.1 The methodology	13
4.1 The relationship between air inlet velocity and seawater velocity	14
4.2 Seawater velocity profile in tubular photobioreactor at air inlet velocity = 0.07 m/s (Top view)	15
4.3 Seawater velocity profile in tubular photobioreactor at air inlet velocity = 0.07 m/s (Side view)	16
4.4 The histogram performs the percentage by weight of fluid in the different velocity ranges of standard U-bend	16
4.5 The histogram performs the percentage by weight of fluid in the different velocity ranges of standard 90 degree bend	17
4.6 (a) Seawater velocity profile,(b) Pressure profile at U-bend	18
4.7 (a) Seawater velocity profile,(b) Pressure profile at 90 degree bend	18
4.8 Vector of seawater flow inside the U-bend	19
4.9 The seawater velocity profile around type 1 of U-bend	20
4.10 The seawater velocity profile around type 2 of U-bend	20
4.11 The seawater velocity profile around type 3 of U-bend	21
4.12 The seawater velocity profile around type 4 of U-bend	21
4.13 The seawater velocity profile around type 5 of U-bend	22
4.14 The seawater velocity profile around type 6 of U-bend	22
4.15 Vector of seawater flow inside the 90 degree bend	24
4.16 The seawater velocity profile around type 1 of 90 degree bend	25
4.17 The seawater velocity profile around type 2 of 90 degree bend	25
4.18 The seawater velocity profile around type 3 of 90 degree bend	26
4.19 The seawater velocity profile around type 4 of 90 degree bend	26
4.20 The relationship between air inlet velocity and seawater velocity	28
4.21 The comparison of air inlet velocity that used in the basic tubular photobioreactor and the optimal tubular	28
4.22 The relationship between air inlet velocity and energy input	29

A.1	Basic tubular photobioreactor	34
A.2	Bend of basic tubular photobioreactor (a) U-bend (b) 90 degree bend	35
A.3	Type 1 of U-bend configuration	35
A.4	Type 2 of U-bend configuration	35
A.5	Type 3 of U-bend configuration	36
A.6	Type 4 of U-bend configuration	36
A.7	Type 5 of U-bend configuration	36
A.8	Type 6 of U-bend configuration	36
A.9	Type 1 of 90 degree bend configuration	37
A.10	Type 2 of 90 degree bend configuration	37
A.11	Type 3 of 90 degree bend configuration	37
A.12	Type 4 of 90 degree bend configuration	37
B.1	The percentage by weight of fluid in the different velocity ranges of type 1 of U-bend	39
B.2	The percentage by weight of fluid in the different velocity ranges of type 3 of U-bend	39
B.3	The percentage by weight of fluid in the different velocity ranges of type 4 of U-bend	40
B.4	The percentage by weight of fluid in the different velocity ranges of type 5 of U-bend	40
B.5	The percentage by weight of fluid in the different velocity ranges of type 6 of U-bend	41
B.6	The percentage by weight of fluid in the different velocity ranges of type 1 of 90 degree bend	41
B.7	The percentage by weight of fluid in the different velocity ranges of type 2 of 90 degree bend	42
B.8	The percentage by weight of fluid in the different velocity ranges of type 3 of 90 degree bend	42
B.9	The percentage by weight of fluid in the different velocity ranges of type 1 of 90 degree bend	43
D.1	Loading file method	48
D.2	Specify multiphase model method	48
D.3	Specify viscous model method	49
D.4	Create material method	49
D.5	Phase set up method	50
D.6	Inlet boundary condition of mixture set up method	50
D.7	Inlet boundary condition of air set up method	51
D.8	Outlet boundary condition of mixture set up method	52
D.9	Outlet boundary condition of air set up method	52
D.10	Operating condition set up method	52
D.11	Region adaption method	53
D.12	Solution initialization method	54

## NOMENCLATURES

$P$	=	Pressure in fluid (Pa)
$P_{\text{loss}}$	=	Pressure loss (Pa)
$W_{\text{loss}}$	=	Energy loss per mass (J/kg)
$\rho$	=	Density of the fluid ( $\text{kg/m}^3$ )
$v$	=	Flow velocity (m/s)
$g$	=	Acceleration of gravity ( $\text{m/s}^2$ )
$h$	=	Elevation (m)
$P_G$	=	Energy input due to aeration (J/s)
$Q_G$	=	Volumetric flow rate of gas ( $\text{m}^3/\text{s}$ )

# CHAPTER 1 INTRODUCTION

## 1.1 Background

Microalgae use carbon dioxide (CO<sub>2</sub>) as a carbon source to grow. They convert CO<sub>2</sub> that increases every day and causes global warming to biomass for bio-refinery such as ethanol, methanol, methane and especially biodiesel. Microalgae are the only one source of renewable biodiesel which has the potential to completely replace petro diesel that is continuously rising in price. Moreover, microalgae also have other advantages as a source of animal feeds and health products. Thus, the cultivation of microalgae has received much attention.

Microalgae cultivation can operate in two systems; the open systems such as raceway and closed systems such as photobioreactors. However, closed photobioreactors offer a better control of the cultivating condition and provide opportunities for culture of a greater variety of algae than is possible in open systems.

Many types of photobioreactors have been designed for microalgae cultivation. One type of them is the tubular photobioreactor which has a potential for large-scale culture of microalgae and is a suitable type for outdoor mass culture. Design parameters of the tubular photobioreactor concerns about efficiently collecting the solar radiation, occupy minimal area to reduce the land demand and especially minimize resistance to flow. If the flow resistance can be minimized, the pressure loss will decrease also. One of methods to decrease the resistance of flow is to modify the configuration of the tubular photobioreactor. Therefore, the study of this research is about the design of the optimal configuration of 90 degree bends and U-bends of the tubular photobioreactor in order to reduce the dead zone and the pressure loss while keeping the turbulent flow in the tube to prevent biomass settling.

## 1.2 Objective

To modify the basic tubular photobioreactor geometry in order to reduce the dead zone and the pressure loss while maintains the turbulent flow in the tube and algal cells in suspension.

## 1.3 Scope of work

1. Simulate the flow behavior inside the tubular photobioreactor in order to predict flow velocity, the pressure loss, the dead zone and the suspension of algal cells by using Computational Fluid Dynamics (CFD) program.
2. Design an optimal configuration of two types of bends which are 90 degree bend and U-bend to reduce the dead zone and the pressure loss.
3. Find the minimum required air inlet velocity that keeps seawater as turbulent flow and algal cell in suspension.

## CHAPTER 2 THEORY AND LITERATURE REVIEWS

This chapter consists of theories and literature reviews about the fundamental data of algae and algae cultivation, photobioreactors and the design criteria of the tubular photobioreactor. Moreover, the mechanical energy balance that is used for calculating the pressure loss in this research and the basic information of Computational fluid dynamics (CFD) program are shown in this chapter

### 2.1 Algae [1,2]

Algae are photosynthetic organisms that mostly found in the marine and freshwater. They convert carbon dioxide and water to oxygen and sugar through the photosynthesis like plants. However, one kind of algae such as Cyanobacteria (blue - green algae) is classified as bacteria because of lacking a membrane-bounded nucleus. Algae have many different sizes ranging from single cells to complex multicellular forms. The most complex algae are called seaweeds. The algae are divided into 2 main types based on the algae body sizes which are microalgae and macroalgae.



**Figure 2.1** Cyanobacteria (blue - green algae) [1]

Macroalgae have the larger cells and can easily be recognizable as plants. Because of the larger size, macroalgae can be harvested more easily. However, macroalgae produce small amounts of lipids, or natural oils, which can be converted into fuel. The cells of microalgae have a variety of forms and colors such as green, blue, red and brown. The most common types can be divided into three groups which consist of Chlorophyta (green), Rhodophyta (red) and Phaeophyta (brown-kelps).



**Figure 2.2** Phaeophyta (brown-kelps) and Rhodophyta (red) [1]

Microalgae are small algae that have to use a microscope to observe. Many microalgal species occur as solitary cells. There are variety cell shapes. The familiar one is small round balls, which look like coccus bacteria, known as coccoid algae. They live in the sea, estuary and on mud. Coccoid cells lack distinct cell wall, but a large quantity of mucilage cover the cell. Another common type of algae body is filament. Filaments are a linear array of cells joined end-to-end, and often sharing a common wall. If the filaments compose of a single row of cells, they are called uniseriate and if the filaments compose of two or more rows of cells, they are described as biseriate or pluriseriate filaments. Microalgae are more favor for cultivating because they grow up very quickly and have much higher lipid content, closed to 60% of their biomass. Thus, the cultivation of microalgae with high oil productivities is desired for biodiesel production.

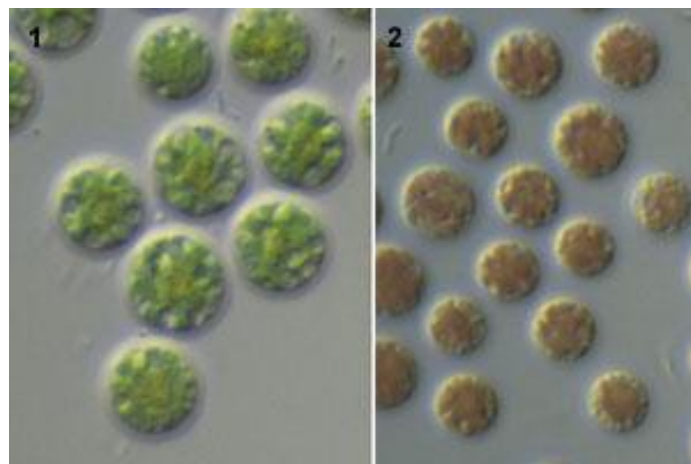


**Figure 2.3** Coccoid algae

(Source: [http://www.shigen.nig.ac.jp/algae\\_tree/Porphyridiophyceae.html](http://www.shigen.nig.ac.jp/algae_tree/Porphyridiophyceae.html))

## 2.2 Algae cultivation systems [3]

The fundamental of algae cultivation related to the photosynthetic reaction which is performed by the chlorophyll that contain in the algae's cells. They take carbon dioxide, water, and sunlight and then convert them into oxygen and sugar as shown in equation 2.2.1



The algae cultivation can be operated in either opened systems or closed systems.

### 2.2.1 Open system

Open-air cultivation systems consist of natural and artificial ponds. They can be also called the inclined surface systems driven by paddle wheels and usually operating at water depths of 15–30 cm. The most common type of open systems is raceway ponds. A raceway pond contains a closed loop recirculation channel that is normally deep about 0.1- 0.3 m and the pond areas are limited about 10,000 m<sup>2</sup> as shown in Figure 2.4. Nutrient fertilizer is added and mixed by a paddle wheel. Mixing of biomass and the growth media is achieved through a combination of the effects of the paddlewheel and the interaction of the water flow with the bottom and sides of the raceway.

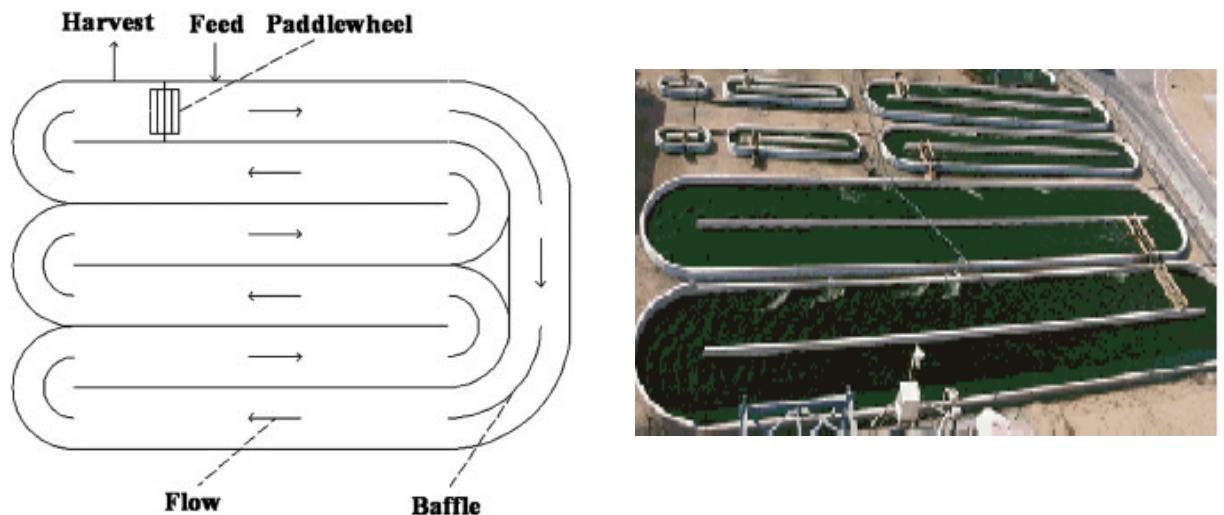


**Figure 2.4** Aerial schematic view of a raceway pond

(Source: <http://vetikaenergia.ee/10600>)

The advantage of open systems is low production costs for algae biomass. In contrast, there are 3 main disadvantages as following 1) a large area is required, 2) there are small numbers of algae species can be grown in the large scale effectively, and 3) the biomass productivity is less than by closed systems.

## 2.2.2 Closed system

Closed loop photobioreactors are developed from open pond systems. The cultivating conditions of closed photobioreactors can be controlled better and they also provide the opportunities for culture of a greater variety of algae than that is possible in open system. Moreover, the photobioreactors have been used successfully for producing large quantities of microalgal biomass. There are many types of photobioreactors that were divided according to the design configurations such as flat-plate photobioreactor, bubble column photobioreactor and tubular photobioreactor.

### 2.2.2.1 Flat-plate photobioreactor [4]

A Flat-plate photobioreactor consists of vertical or inclined rectangular boxes that are often divided in two parts to affect a mix of the reactor fluid. The culture in this photobioreactor is mixed with air that is introduced at the bottom of the reactor. The optimum large scale flat plate photobioreactor module is 1000 m<sup>2</sup> while a commercial capacity is 6000 L [5].

In general, the flat-plate photobioreactors are made of transparent materials for the maximum utilization of solar light energy. The major advantages of flat-plate photobioreactors are the high productivity and efficiency in utilizing solar energy because of the high area-to-volume ratio. Moreover, the accumulation of dissolved oxygen is lower than the tubular photobioreactors. However, there is limitation of controlling culture temperature. In addition, the scale-up step requires many compartments and support materials.

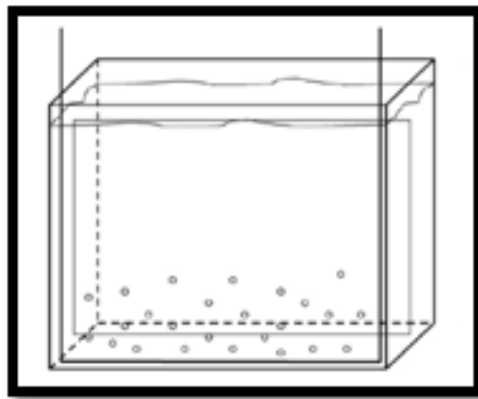


**Figure 2.5** Flat-plate photobioreactor

(Source: [http://www.ask.com/wiki/Algae\\_bioreactor](http://www.ask.com/wiki/Algae_bioreactor))

### 2.2.2.2 Bubble column photobioreactor

A bubble column contains vertical arranged cylindrical column. It is made of transparent materials. The maximum of column diameter is limited about 20 to 30 cm to ensure the sufficient supply of sunlight energy. Gas is fed into the column at the bottom.

The bubble column photobioreactors have many advantages such as good mixing with low shear stress, easy to sterilize, high mass transfer and low energy consumption. On the other hand, the drawbacks are small illumination surface area and required sophisticated materials for their construction.

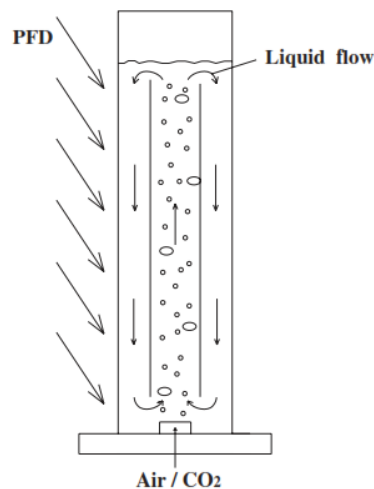


**Figure 2.6** Bubble column photobioreactor [3]

(Source: [http://www.ask.com/wiki/Algae\\_bioreactor](http://www.ask.com/wiki/Algae_bioreactor) )

### 2.2.2.3 Tubular photobioreactor[3,6]

A tubular photobioreactor consists of an array of straight, coiled, or looped tubes that are made of transparent plastic or glass as shown in Figure 2.7 [7]. The cultures are circulated through the tubes by a pump, or an airlift device [8]. The airlift technology is more effective as the following reasons: (1) the circulation is accomplished without moving parts (2) the cell damage that associated with mechanical pumping is minimized and airlift device combines the function of a pump and a gas exchanger that removes the oxygen produced by photosynthesis.

A fully closed tubular photobioreactor is suitable for the large-scale culture of microalgae and is one of the more suitable types for outdoor mass culture. The main disadvantages of this reactor are the deficiency of carbon dioxide and the high concentration of oxygen at the end of the unit during the circulation.



**Figure 2.7** Tubular photobioreactor

(Source: <http://www.ncrisbiofuels.org/facilities>)

### 2.3 Criteria of the tubular photobioreactor design [6,7,12]

An airlift driven tubular photobioreactor is shown in Figure 2.8. There are 2 main parts which are the solar collector tube as shown in Figure 2.8(a) and the airlift system as shown in Figure 2.8(b)

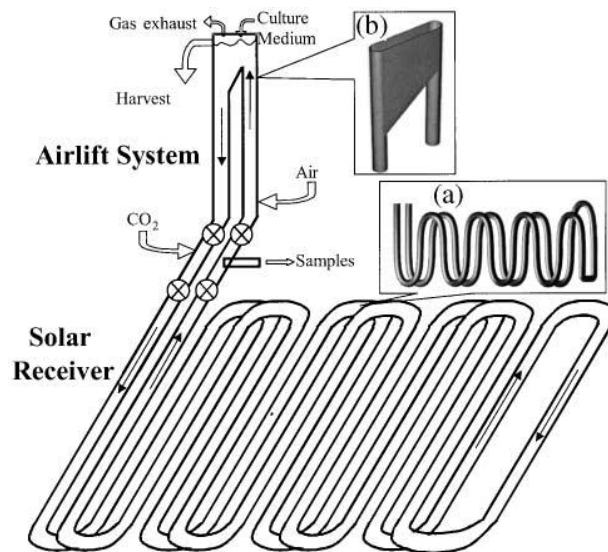


**Figure 2.8** Tubular photobioreactor with details of (a) the solar loop and (b) the degasser zone [7]

The airlift device circulates the culture through the solar collector tubing where most of the photosynthesis occurs. From the review on previous research [6,7], the design of a tubular photobioreactor focuses on the airlift column and solar collector separately. The volume of airlift device must be smaller than the volume of the solar collector loop so that the cells spend less time in the darker region of this reactor. The head zone of the airlift column is designed for almost complete separation of the gas from the liquid, before the fluid recirculated into the solar collector.

For the good solar collective design, it should have the effective solar radiation collector, the occupied minimal area to reduce the land demand and especially the minimum resistance to flow. The tube length of the solar collector loop is limited in cases of too long the tubes produced the accumulated oxygen by photosynthesis. The oxygen will accumulate in the broth until the fluid returns to the airlift zone where the accumulated oxygen is stripped by air. This removal oxygen is very important because excessive dissolved oxygen in the culture inhibits the photosynthesis. The oxygen concentrations above 35 mg/L are toxic to most microalgae. In addition, the diameter of tube is limited also since the increasing tube diameter results in a decrease in the surface-to-volume ratio (i.e., the ratio between the illuminated surface of a reactor and its volume) which affect on the cultivation. Generally, the tube diameter is limited at 0.1 m.

Besides the surface-to-volume ratio and the oxygen accommodation, the mixing is the one of the factors that needs to be considered for the photobioreactor design. There are many roles of the mixing that are to ensure light intensity distribution, to avoid the thermal stratification, to transfer  $\text{CO}_2$  sufficiently and to maintain uniform pH [13]. Mixing also ensures that all cells are equally exposed to the light and nutrients and improves gas exchange between the culture medium and the air [14]. Moreover, the mixing necessary to prevent the sedimentation of cells at the same time avoid the cells attachment to the reactor wall. Poor mixing will allow agglutination of cells into aggregates of various sizes. However, high mixing rates may lead to shear induced damage of cells which may also harm their viability [15].

## 2.4 Mechanical Energy Balance [16]

The mechanical energy consists of the kinetic energy, the potential energy, the flow work and the work terms. They are the forms of energy that can be directly converted to the work. The mechanical energy balance for an incompressible fluid and a steady state system can be proved by following these steps.

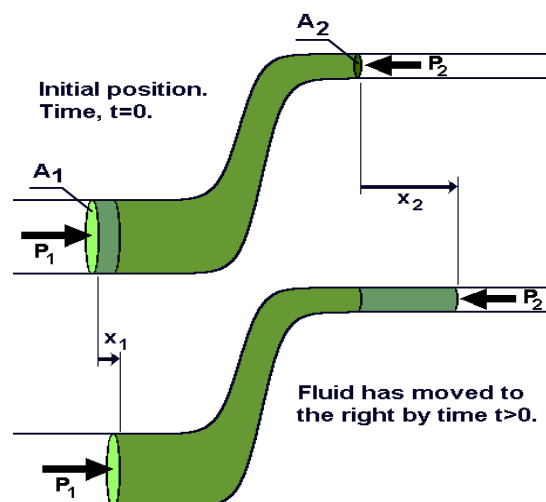


**Figure 2.9** The position of fluid flow at time  $\geq 0$  [16]

The fluid section of mass ( $m$ ) is moved to the right as shown in Figure 2.9. The net work done in moving the fluid is

$$\Delta W_{1 \rightarrow 2} = W_1 + W_2 - W_{loss} \quad (2.4.1)$$

$$\Delta W_{1 \rightarrow 2} = F_1 \times X_1 - F_2 \times X_2 - W_{loss} \quad (2.4.2)$$

Where  $F$  is a force and  $X$  is a displacement. The second term picked up its negative sign because the force and displacement are in opposite directions.  $W_{loss}$  represents the mechanical energy loss that may occur due to the friction.

Pressure is the force exerted over the cross-sectional area that you can write in term of  $P = \frac{F}{A}$ . Rewrite this as  $F = PA$  and substitute into equation (2.4.2)

$$\Delta W_{1 \rightarrow 2} = P_1 \times A_1 \times X_1 - P_2 \times A_2 \times X_2 - W_{loss} \quad (2.4.3)$$

The displaced fluid volume  $V$  is the cross-sectional area  $A$  times the thickness  $X$ . This volume remains constant for an incompressible fluid; Therefore,

$$V = A_1 \times X_1 = A_2 \times X_2 \quad (2.4.4)$$

From equations (2.4.3) and (2.4.4), it can be written to

$$\Delta W_{1 \rightarrow 2} = (P_1 - P_2)V - W_{loss} \quad (2.4.5)$$

Since work has been done, there has been a change in the mechanical energy of the fluid segment as shown in Figure 2.10

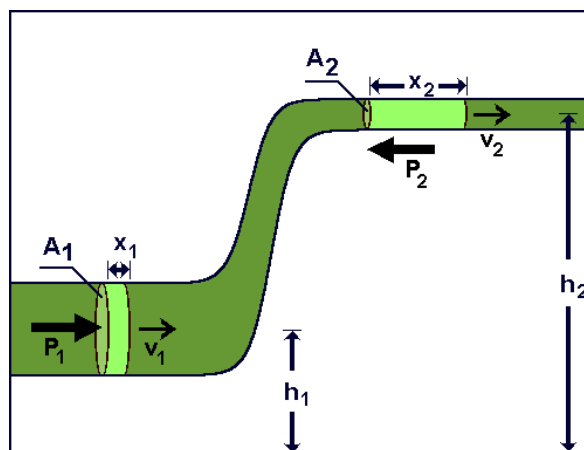


**Figure 2.10** The control volume of fluid flow system [16]

The energy change between the initial and final positions is given by

$$\Delta E = E_2 - E_1 = (U_2 + K_2) - (U_1 + K_1) \quad (2.4.6)$$

Where  $K$  is the kinetic energy and  $U$  is the potential energy. Thus, it can be rewritten as shown in equation (2.4.7)

$$\Delta E = \left( mgh_2 + \frac{mv_2^2}{2} \right) - \left( mgh_1 + \frac{mv_1^2}{2} \right) \quad (2.4.7)$$

Where  $m$  is the fluid mass,  $v$  is the speed of the fluid,  $g$  is the acceleration of gravity and  $h$  is average fluid high.

The work-energy theorem says that the net work done is equal to the change in the system energy. This can be written as

$$\Delta E = \Delta W \quad (2.4.8)$$

Finally, substitution of Equation (2.4.5) and Equation (2.4.7) into Eq.(2.4.8). You will get the mechanical energy balance as shown in equation (2.4.9)

$$(P_1 - P_2)V - W_{loss} = \left( mgh_2 + \frac{mv_2^2}{2} \right) - \left( mgh_1 + \frac{mv_1^2}{2} \right) \quad (2.4.9)$$

Or, it can be written in the form of the pressure loss by dividing Eq.(2.4.9) by the fluid volume,  $V = \frac{m}{\rho}$  as shown in equation (2.4.10)

$$(P_1 - P_2) - P_{loss} = \left( \rho gh_2 + \frac{\rho v_2^2}{2} \right) - \left( \rho gh_1 + \frac{\rho v_1^2}{2} \right) \quad (2.4.10)$$

$$\text{Or,} \quad \rho gh_1 + \frac{\rho v_1^2}{2} + P_1 = \rho gh_2 + \frac{\rho v_2^2}{2} + P_2 + P_{loss} \quad (2.4.11)$$

Where  $p$  = pressure in fluid (Pa (N/m<sup>2</sup>), psi (lb/ft<sup>2</sup>))  $p_{loss}$  = pressure loss (Pa (N/m<sup>2</sup>), psi (lb/ft<sup>2</sup>))

$\rho$  = density of the fluid (kg/m<sup>3</sup>, slugs/ft<sup>3</sup>)       $v$  = flow velocity (m/s, ft/s)

$g$  = acceleration of gravity (m/s<sup>2</sup>, ft/s<sup>2</sup>)       $h$  = elevation (m, ft)

In the energy balance, there is a term  $P$  that appears in balance term associated with each inlet or outlet. This term is actually a flow work term that results from the work which must be done to push a packet of fluid into or out of the system as shown in the proved method above.

The mechanical energy balance can be used for calculating the pressure drop along the tube of the tubular photobioreactor in this research.

## **2.5 Computational fluid dynamics (CFD) [12]**

Computational fluid dynamics is an efficient tool to study the fluid flows. This tool is a numerical technique for the solution of the equations governing the flow of fluid inside geometry. A prediction of the fluid dynamics and the related physical phenomena can be determined by CFD. The flow of any fluid can be described using the Navier's stokes transport equations [17]. These equations are derived by considering mass, momentum and energy balances in an element of fluid, resulting in a set of partial differential equations. They can be completed by additional of other algebraic equations from thermodynamics such as the equation of state for density and a constitutive equation to describe the rheology.

### **2.5.1 Flow modeling**

There are two categories of flow model.

#### **2.5.1.1 Turbulent modeling**

Turbulence modeling is a key issue in most CFD simulations. In the photobioreator, the growth rates of some microalgae increase initially with increasing turbulence. However, the growth decreases sharply with further increase of the gas velocity due to cell [18]. Many factors such as the grid resolution and the selection of the turbulence model are very important in order to obtain accurated prediction of hydrodynamics in the PBR [19]. In two phase flows simulations, the  $k-\epsilon$  turbulence model published by Launder and Spalding [20] has been widely used because of its simplicity and its capability for prediction of wall-bounded turbulent flows [21]

There are three different options available for turbulence modeling of multiphase flow in FLUENT software which are the mixture  $k-\epsilon$ , dispersed  $k-\epsilon$  and two-phase  $k-\epsilon$  models [22]. All three turbulence models used the same model constants but have different equations to account for the turbulence viscosity [19].

#### **2.5.1.2 Species modeling**

Among the available multiphase simulation approaches for hydrodynamic studies, the Eulerian–Eulerian, Lagrangian–Eulerian and the Volume of Fluid (VOF) multiphase models have been generally used. The species transport in multiphase models solves the conservation equations describing convection, diffusion, and reaction sources for each component species. Multiple simultaneous chemical reactions can be modeled, with reactions occurring in the bulk phase (volumetric reactions) and/or on wall or particle surfaces, and in the porous region.

## **CHAPTER 3 METHODOLOGY**

The aim of this thesis is the modification of the basic tubular photobioreactor geometry in order to minimize the pressure loss while keeping the turbulent flow in the tube to prevent the sedimentation of algae cells. The steps of work which is used to achieve this thesis consists of 4 main steps as shown in Figure 3.1. In addition, the detail of each step is described in this chapter as well.

### **3.1 Information preparation**

In the first step, all information related to the algae cultivation and the tubular photobioreactor including the calculation method of the pressure loss along the tube was studied by searching and gathering from relevant internet, text books, and literature.

### **3.2 Basic tubular photobioreactor model and the simulation by using CFD**

The basic geometry of the tubular photobioreactor based on the provided configuration as shown in Appendix A was drawn and meshed by using ICEM CFD program. Then, FLUENT is used to simulate the flow behavior inside the tubular photobioreactor and to calculate simulation results. FLUENT requirements are the tubular photobioreactor geometry, the boundary conditions, material, models etc. After that, the simulation results is analyzed in order to predict the pressure loss, the flow velocity, the dead zones and the suspension of algae cells by using CFD Post-Process program. Air inlet velocity will be varied from 0.05 to 0.1 m/s to find the optimal air velocity. Furthermore, the pressure loss of the basic tubular photobioreactor is also calculated in this step. The method to set the model in FLUENT software including boundary condition and material is summarized Appendix C.

### **3.3 Optimization of the bend configuration of the tubular photobioreactor**

Refer to the base case simulation; the basic geometry of the tubular photobioreactor will be modified by designing the configuration of the bends in order to reduce the dead zone and the pressure loss. FLUENT software was used for the new configurations. Then, the minimum flow velocity to maintain the turbulent flow, the suspension of algae cells, and to handle the pressure loss of each configuration are expressed. The pressure loss results from all configurations are compared and then the optimal configuration of the tubular photobioreactor which can reduce more dead zone and pressure loss was selected.

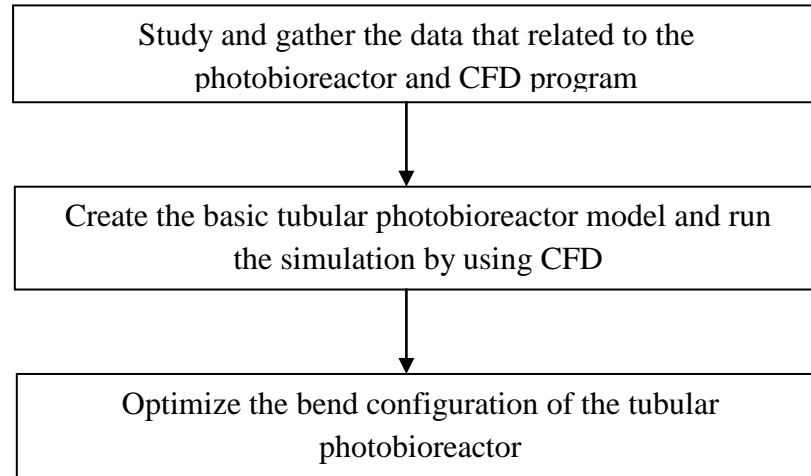


**Figure 3.1** The methodology

## CHAPTER 4 RESULTS AND DISCUSSION

This chapter contains the simulation results and discussion. It is divided into 3 main sections. The first section shows a base model of the tubular photobioreactor which consists of the velocity profile and the pressure loss of 90 degree bend and U-bend calculation. In addition, the velocities of air and seawater will be considered to find the minimum air velocity that keeps the seawater velocity as turbulent flow. The second section studies the optimal configuration of bends of the tubular photobioreactor to eliminate the dead zones with uniform velocity and reduce the pressure loss. New bend configurations were proposed and the result of each case was compared in this section. The last section shows the simulation result of the optimal tubular photobioreactor including the comparison with the base model.

### 4.1 Base model of the tubular photobioreactor

The base model of the tubular photobioreactor refers to the provided configuration. Three main issues need to be considered in this section. First is the effect of air velocity on the seawater velocity. Second are the positions of the dead zones. Last is the pressure loss of 90 degree bend and U-bend.

#### 4.1.1 Effect of air velocity on the seawater velocity

Air flow rate affects the energy input. If the air flow rate increases, the energy input will increase. Therefore, the relationship between air velocity and seawater velocity shown in Figure 4.1 needs to be considered in order to find the minimum air velocity to reduce the energy consumption while the seawater is still turbulent flow ( $Re \geq 10,000$ ). Air velocity was varied between 0.05 to 0.1 m/s.

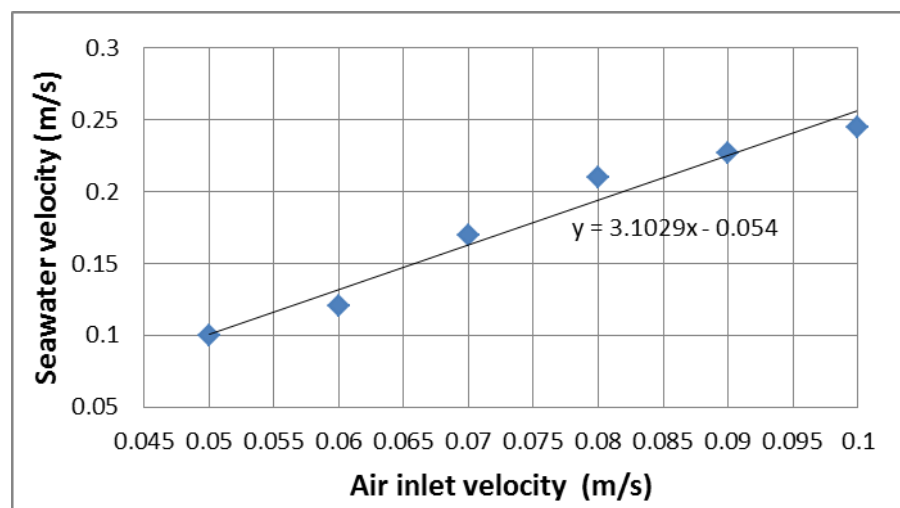


**Figure 4.1** The relationship between air inlet velocity and seawater velocity

As seen in this figure, both air and seawater velocities have a linear relationship. Seawater velocity will decrease with the decreasing of air velocity. The minimum seawater velocity for turbulent flow to prevent the algal cell settling is 0.1 m/s ( $Re \approx 10,000$ ) which needs the air inlet velocity equals to 0.05 m/s.

However, an oxygen accumulation increases at lower seawater velocity in the solar tube. Generally, the acceptable lowest flow velocity is 0.17 m/s [8]. If the flow velocity is lower than 0.17 m/s, the dissolved oxygen concentration approaches at 300% of air saturation which makes the culture collapsed by photooxidation effects. Thus, the suitable air inlet velocity for this reactor is 0.072 m/s.

#### 4.1.2 Velocity profile of base model

Velocity profile of seawater in the tubular photobioreactor at air inlet velocity at 0.07 m/s is shown in Figures 4.2 and 4.3

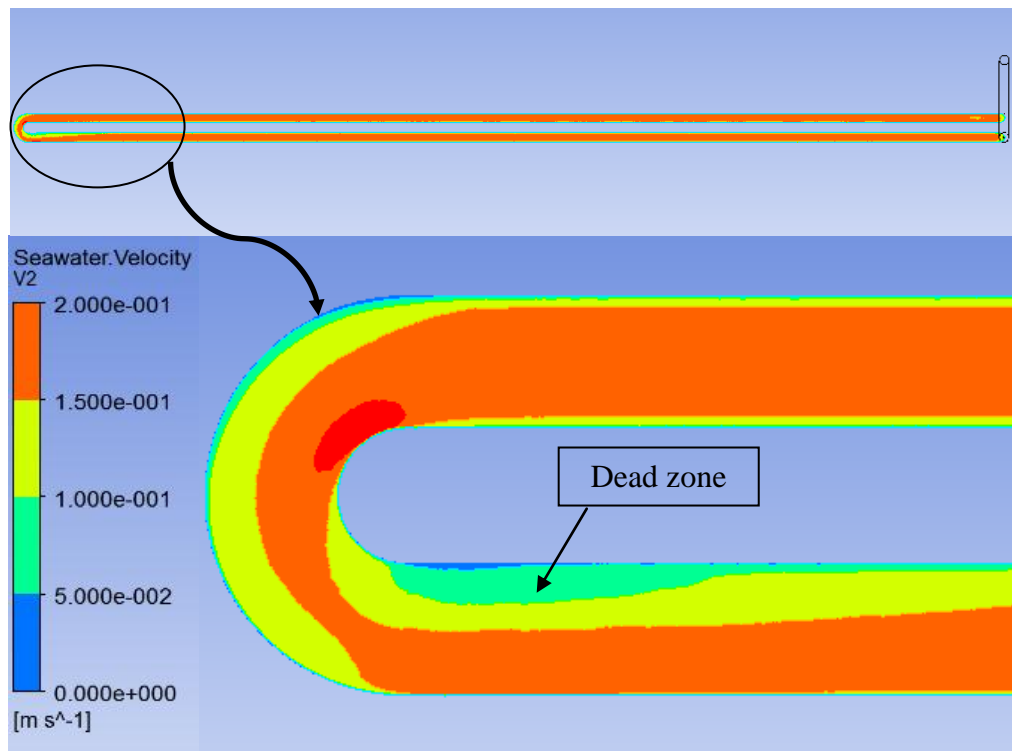


**Figure 4.2** Seawater velocity profile in the tubular photobioreactor at air inlet velocity 0.07 m/s (Top view)

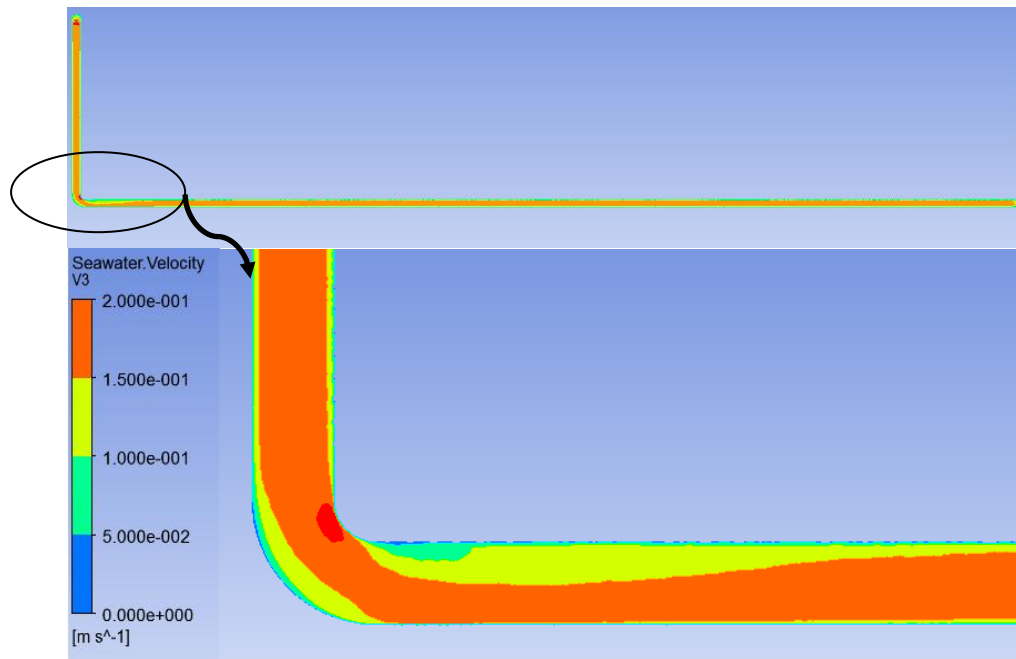


**Figure 4.3** Seawater velocity profile in the tubular photobioreactor at air inlet velocity 0.07 m/s (Side view)

These figures show that seawater velocity at the dead zone is less than 0.1 m/s in green and blue color, appearing after the fluid pass U-bend tube and 90 degree bend, respectively. Moreover, these figures illustrate that the seawater velocity during pass the U-bend tube and the 90 degree bend is not the uniform velocity.

The histogram performs the percentage by weight of fluid in the different velocity ranges is shown in Figures 4.4 and 4.5. Thus, the dead zone can be calculated in terms of quantity.

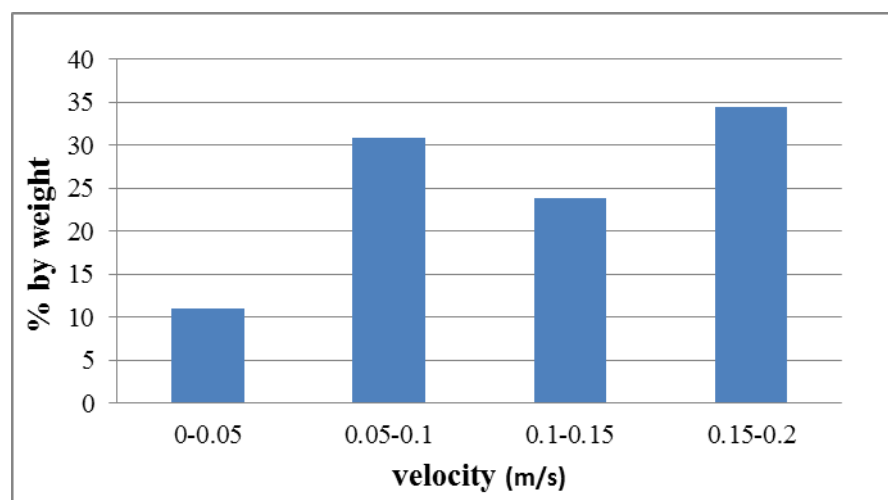


**Figure 4.4** The histogram performs the percentage by weight of fluid in the different velocity ranges of standard U-bend.

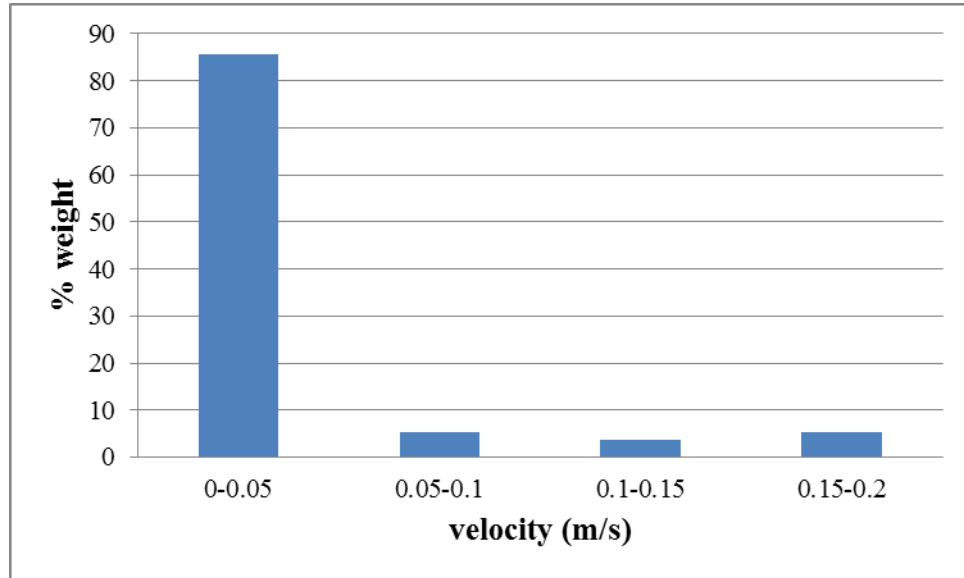


**Figure 4.5** The histogram performs the percentage by weight of fluid in the different velocity ranges of standard 90 degree bend.

The dead zone of U-bend is 41.857% weight and the dead zone of 90 degree bend is 90.94 % weight as shown in Figures 4.4 and 4.5; respectively.

Both the dead zone and the different velocity in the tube are an unacceptable characteristic of the tubular photobioreactor. Hence, the new configurations of bends should be proposed to improve these problems in section 4.2

#### 4.1.3 Pressure loss of bends

Pressure loss across bends can be calculated by mechanical energy balance as shown in equation (4.1.3.1)

$$\rho gh_1 + \frac{\rho v_1^2}{2} + P_1 = \rho gh_2 + \frac{\rho v_2^2}{2} + P_2 + P_{loss} \quad (4.1.3.1)$$

However, this study does not focus on the hydrostatic pressure so the equation (4.1.3.1) can be reduced to equation (4.1.3.2).

$$\frac{\rho v_1^2}{2} + P_1 = \frac{\rho v_2^2}{2} + P_2 + P_{loss} \quad (4.1.3.2)$$

Where  $p$  = pressure in fluid (Pa)

$\rho$  = density of the seawater = 1020 kg/m<sup>3</sup>

$g$  = acceleration of gravity (m/s<sup>2</sup>)

$p_{loss}$  = pressure loss (Pa)

$v$  = flow velocity (m/s)

$h$  = elevation (m)

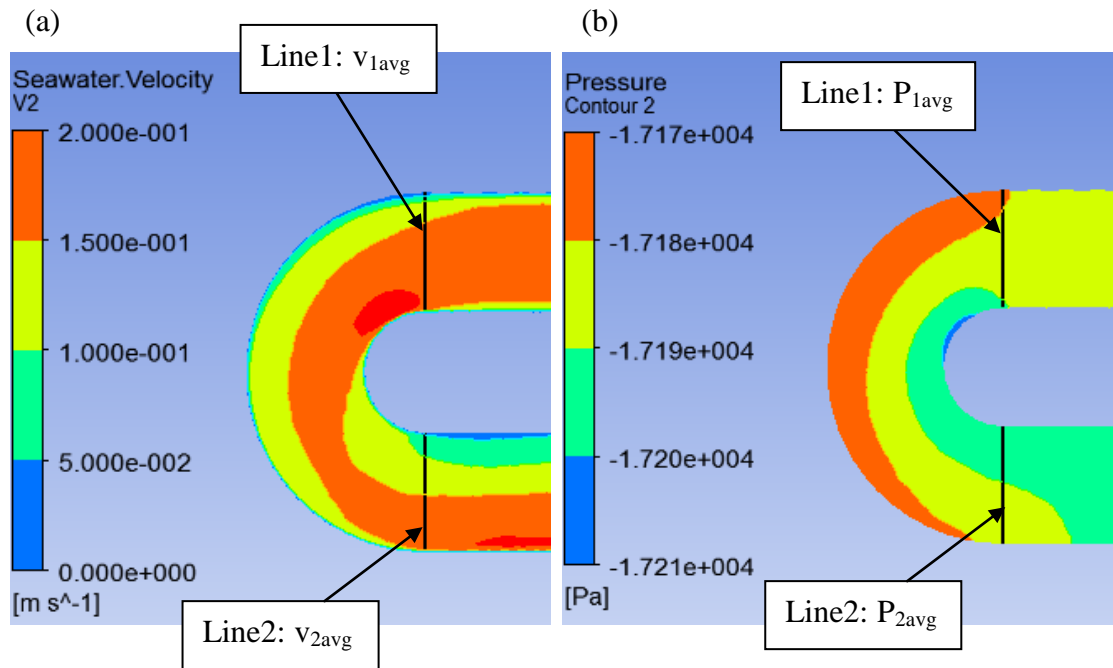


**Figure 4.6** (a) Seawater velocity profile, (b) Pressure profile at U-bend

From equation (4.1.3.2),  $v_1, v_2, P_1$  and  $P_2$  can find from the simulation result. As Figure 4.6,  $v_1$  and  $P_1$  is the average velocity and pressure of line 1 at 0.160 m/s and 27.884 Pa and  $v_2$  and  $P_2$  is the average velocity and pressure of line 2 at 0.157 m/s and 10.457 Pa; respectively. Therefore, the pressure loss across this U-bend tube is 17.920 Pa.

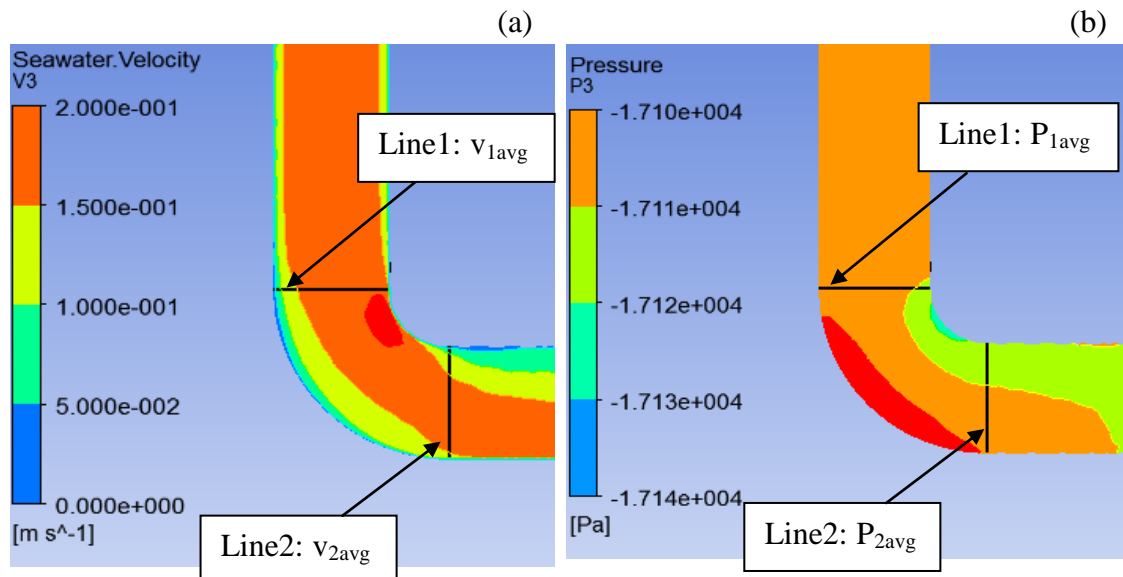


**Figure 4.7** (a) Seawater velocity profile, (b) Pressure profile at 90 degree bend

Figure 4.7 shows the values of  $v_1$  and  $P_1$  are 0.160 m/s and 12.061 Pa and  $v_2$  and  $P_2$  are 0.150 m/s and 7.120 Pa ; respectively. Pressure loss across 90 degree bend calculated by equation (4.1.3.2) is 6.569 Pa

## 4.2 Modified model of the tubular photobioreactor

The basic tubular photobioreactor was simulated and shown the dead zone at 90 degree bend and U-bend and the high pressure loss across the bends. Thus, these bends need to be redesigned in order to decrease the dead zone and the pressure loss around the bends.

There are 3 main criteria that use to select the optimal bend configuration. Firstly, it can eliminate the dead zone. Secondly, the fluid has a uniform velocity when pass through the bend tube. Lastly, it can reduce the pressure loss across bends.

### 4.2.1 U-bend configuration improvement

The base model result showed that the dead zone appeared after the fluid pass U-bend. It can be seen obviously from the vector of seawater flow that seawater does not flow following the bend but trying to flow in straight direction as in Figure 4.8.

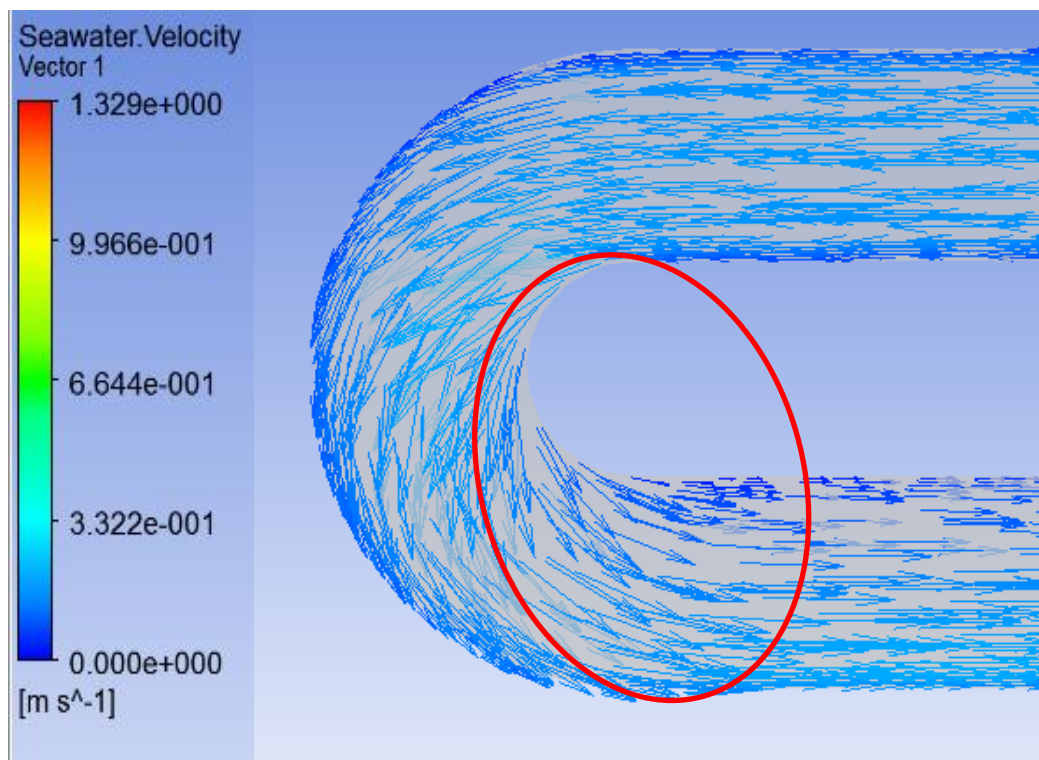


**Figure 4.8** Vector of seawater flow inside the U-bend

According to this problem, U-bend was modified by increasing the radius of curvature and designing the return part of U-bend tube. There are 6 new configurations of U-bend proposed in this research as the detail of the dimension shown in Appendix A.

#### 4.2.1.1 Seawater velocity analysis

First consideration used as a guide to improve the configuration of bend is the seawater velocity profile around the U-bend.

Type 1: This type is modified from the base configuration by increasing the radius of U-bend from 0.1 to 0.15 m. The seawater velocity profile is shown in Figure 4.9

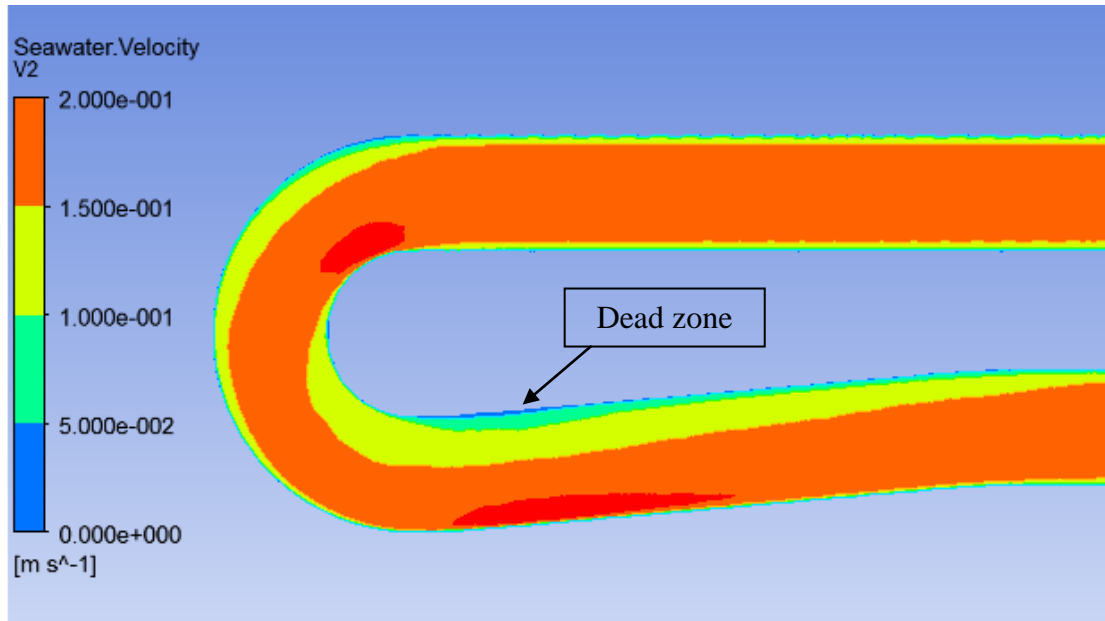


**Figure 4.9** The seawater velocity profile around type 1 of U-bend.

This U-bend type can reduce the dead zone from the base configuration. However, the seawater velocity is still not the uniform velocity when the fluid passed the U-bend tube. Thus, the radius of curvature was increased in the next configuration.

Type 2: This type was increased the radius of U-bend to 0.5 m and used only 5 degree angle to return to the straight pipe.

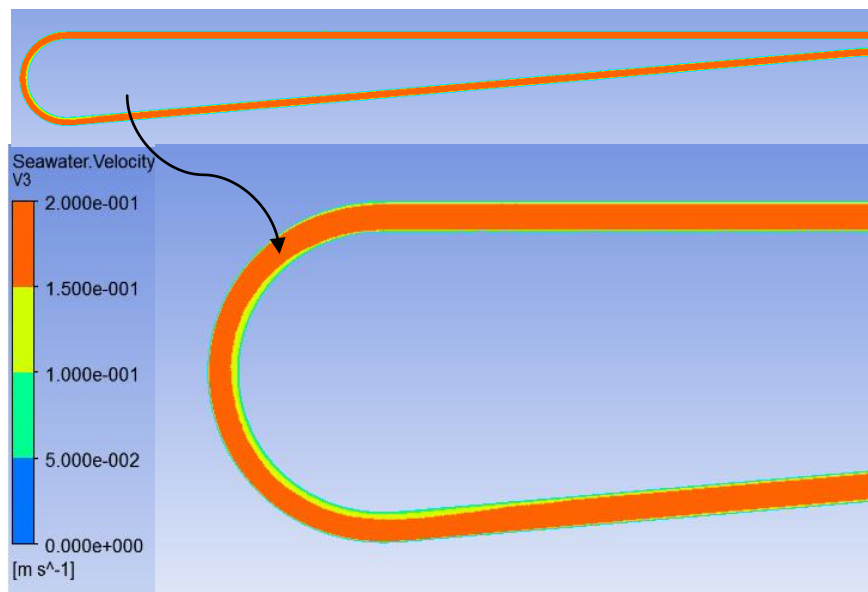


**Figure 4.10** The seawater velocity profile around type 2 of U-bend.

Figure 4.10 shows type 2 of U-bend. It can eliminate the dead zone and make the uniform velocity across u-bend. However, the total length is longer than the base configuration because it uses too long distance to return to the same position of straight pipe. Therefore, this design cannot use in the real construction and next configuration is designed to reduce the return path to the straight pipe.

Type 3: This type uses the same radius as type 2 because it is sufficiency to eliminate the dead zone. However, this type was designed the new return part of U-bend tube by increasing the angle of arc from 180 to 225 degree as shown in Figure 4.11.

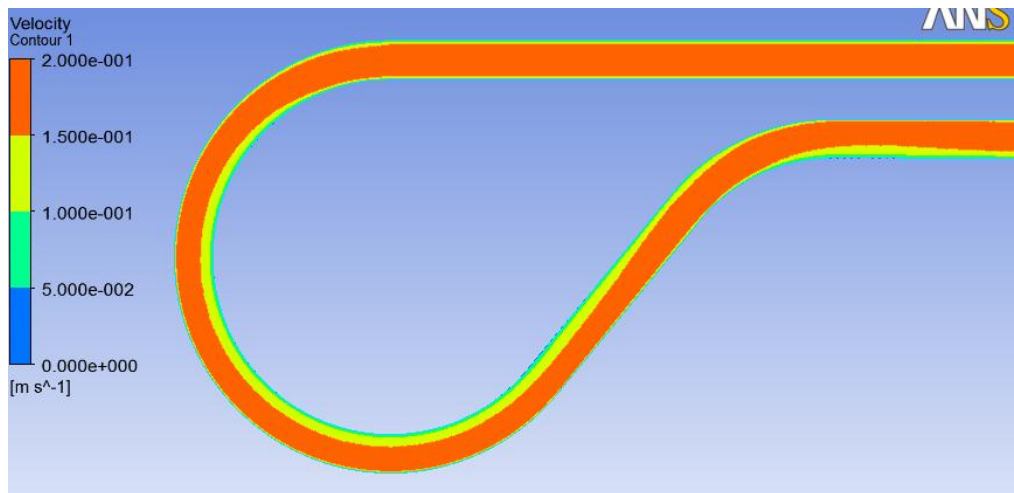


**Figure 4.11** The seawater velocity profile around type 3 of U-bend.

This figure shows that the seawater velocity is more uniform velocity than the base configuration of U-bend and most of the dead zone is eliminated. Nevertheless, the radius of curvature may be smaller than this in order to save the area.

Type 4: This type is similar to the type 3 but use the less radius of curvature which is 0.35 m as shown in Figure 4.12.

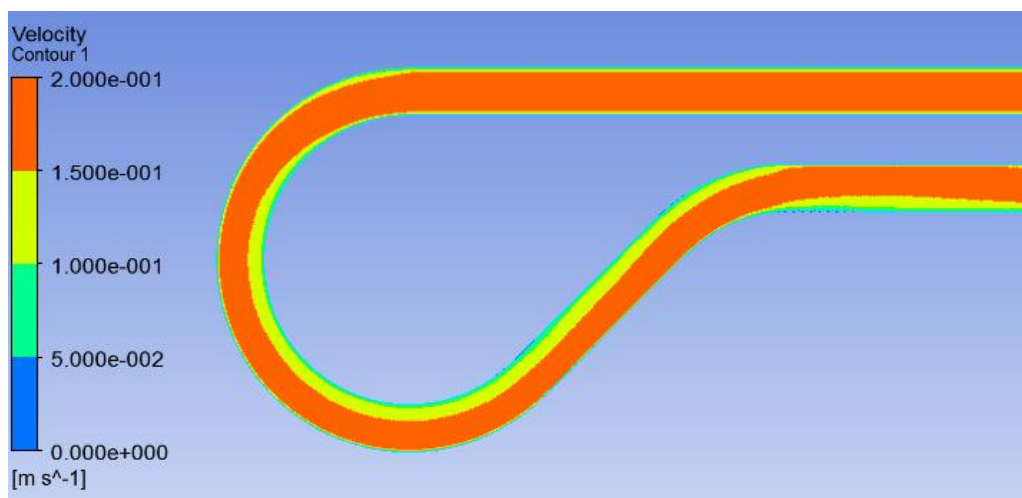


**Figure 4.12** The seawater velocity profile around type 4 of U-bend.

This type can eliminate most dead zone and the velocity is more uniform than the base model. However, it still has the yellow color in the return part of U-bend which means velocity is not completely uniform. The next type was design the return part of U-bend as shown in type 5.

Type 5: This type is similar to type 4 excepting the angle of arc that is decreased to 210 degree. The velocity profile around this U-bend is shown in Figure 4.13.

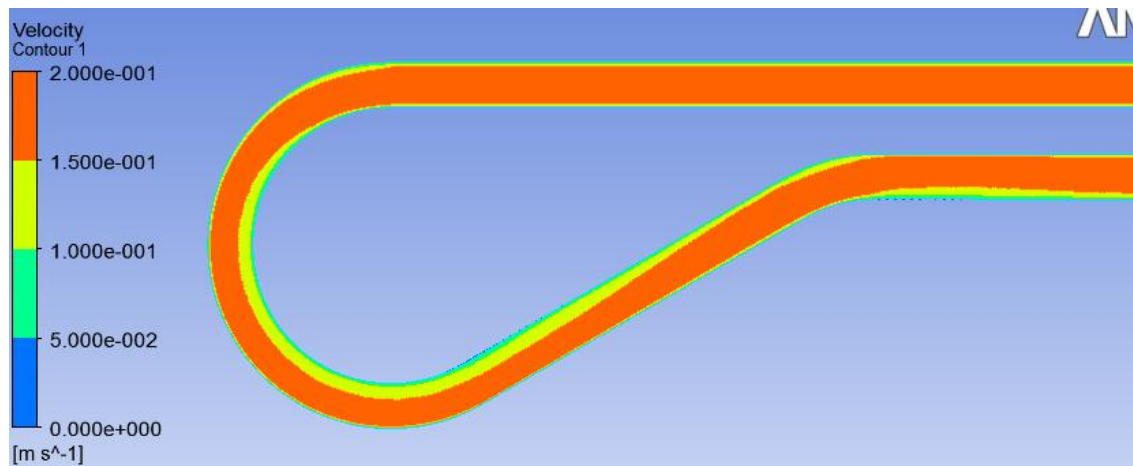


**Figure 4.13** The seawater velocity profile around type 5 of U-bend.

The velocity is more uniform than the other types excepting type 3. Moreover, it can eliminate almost all dead zones so this type may be a suitable one of the configuration of the U-bend. However, next configuration was proposed decrease the radius of curvature of U-bend in order to reduce the space.

Type 6: The radius of curvature of this configuration is 0.25 m and the angle of arc is 225 degree. The velocity profile around the bend of this type is shown in Figure 4.14.

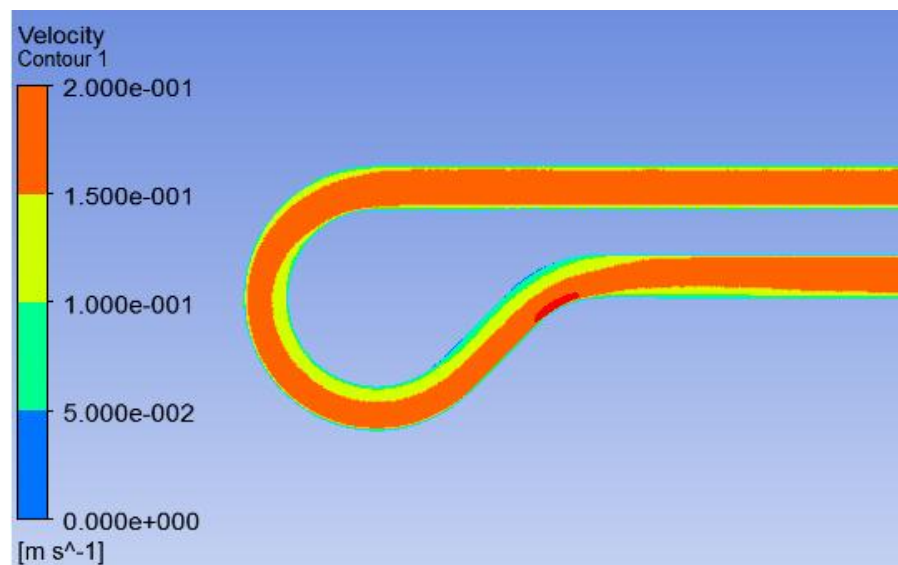


**Figure 4.14** The seawater velocity profile around type 6 of U-bend.

This figure shows that this radius is too small to make the uniform velocity because the velocity profile has much yellow color. However, it can reduce the dead zone from standard U-bend.

All of these are the velocity profile result of the new configurations that were proposed in this research. Table 4.1 concludes of the dead zone percentage of each type which calculates from histograms in Appendix B and the percentage of the dead zone reduction from the standard U-bend.

**Table 4.1** Percentage of the dead zone

Type of U-bend	%Dead zone	%Reduction
Standard	41.857	0
Type 1	38.633	7.703
Type 3	40.357	3.584
Type 4	39.273	6.173
Type 5	<b>37.898</b>	<b>9.459</b>
Type 6	38.025	9.154

Note: - Type 2 is not showed in this table because it cannot construct practically.

From Table 4.1, type 5 of U-bend can reduce the dead zone higher than other types. The dead zone reduces from the standard U-bend by 9.459%.

Referring to three criteria, not only the dead zone and uniform velocity is discussed in this section but also the pressure loss has to be considered. Hence, the pressure loss comparisons of the base case with the other cases are discussed in the section 4.2.1.2.

#### 4.2.1.2 Comparison of Pressure loss

The pressure loss across bend is calculated from equation 4.1.3.2. Pressure loss of each case and the percentage of the pressure loss reduction from the base case are shown in Table 4.2 and the calculation method is shown in Appendix C

**Table 4.2** Pressure loss of each case and percentage of the pressure loss reduction.

U-bend type	$P_{\text{loss}}$	delta $P_{\text{loss}}$	% Reduction
Standard	17.920	0.000	0.000
Type 1	16.511	1.409	7.862
Type 3	16.937	0.984	5.488
Type 4	16.275	1.646	9.183
Type 5	<b>15.674</b>	<b>2.246</b>	<b>12.534</b>
Type 6	16.759	1.161	6.478

\* $P_{\text{loss}}$  is calculated at the same length

The Table 4.1 shows every type of U-bend can reduce the pressure loss from standard U-bend but type 5 of U-bend has the highest reduce percentage of the pressure loss from the base configuration which equals to 12.534%.

According to 3 criteria, type 5 is the optimal configuration of U-bend because it can reduce the highest dead zones and pressure loss and make the uniform velocity.

#### 4.2.2 90 degree bend configuration improvement

The dead zone occurs around the outlet of 90 degree bend. Since the fluid does not flow along the curve as seen from the vector of seawater velocity in Figure 4.15

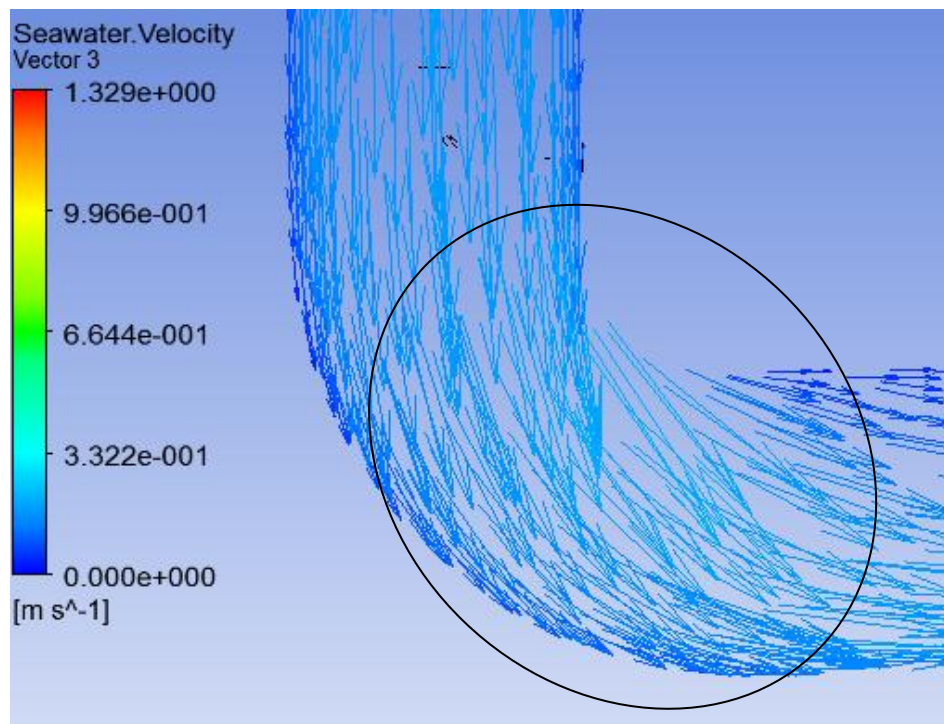


**Figure 4.15** Vector of seawater flow inside the 90 degree bend

There are 4 configurations of 90 degree bend. First one is the sharp 90 degree bend. The other two types are the bend that have the radius of curvature equal to 0.2 m and 0.3 m. The last type is the bend that use 2 angle of 45 degree connected by the straight pipe. The detail of the dimension of bends is shown in Appendix A and the result of the velocity profiles across 90 degree bend are shown in following section.

##### 4.2.2.1 Seawater velocity analysis

The 2 importance things that have to consider from the velocity profile are the dead zone and the uniform velocity around the bend. The velocity profiles of each type of 90 degree bend are shown below.

Type 1: The sharp 90 degree bend.

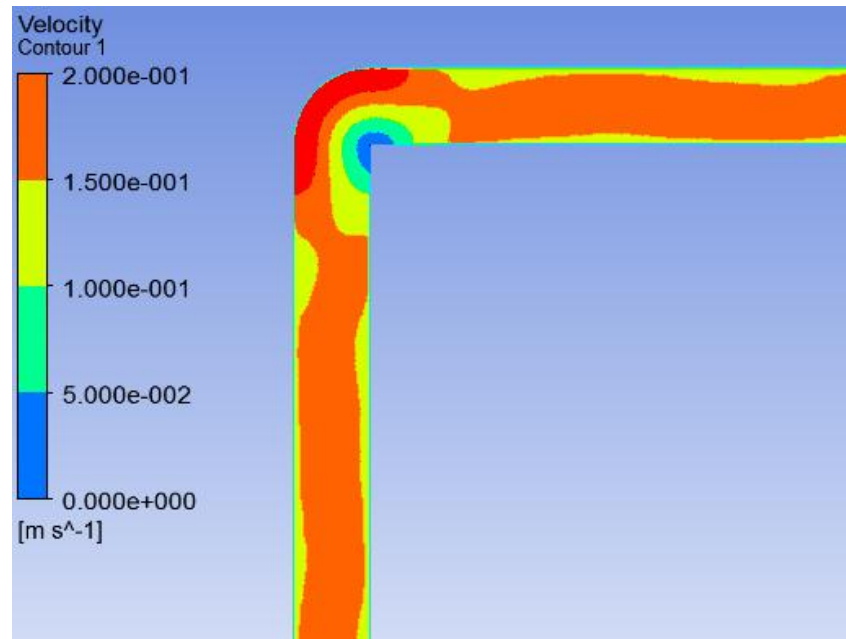


**Figure 4.16** The seawater velocity profile around type 1 of 90 degree bend

As Figure 4.16, the sharp 90 degree bend give the worse result than the base geometry of 90 degree bend. There are the bigger dead zone and un-uniform velocity. Hence, the decreasing of radius is not the suitable way to improve the configuration. Next configuration was designed by increasing the curvature.

Type 2: This type uses the radius curvature of 0.2 m

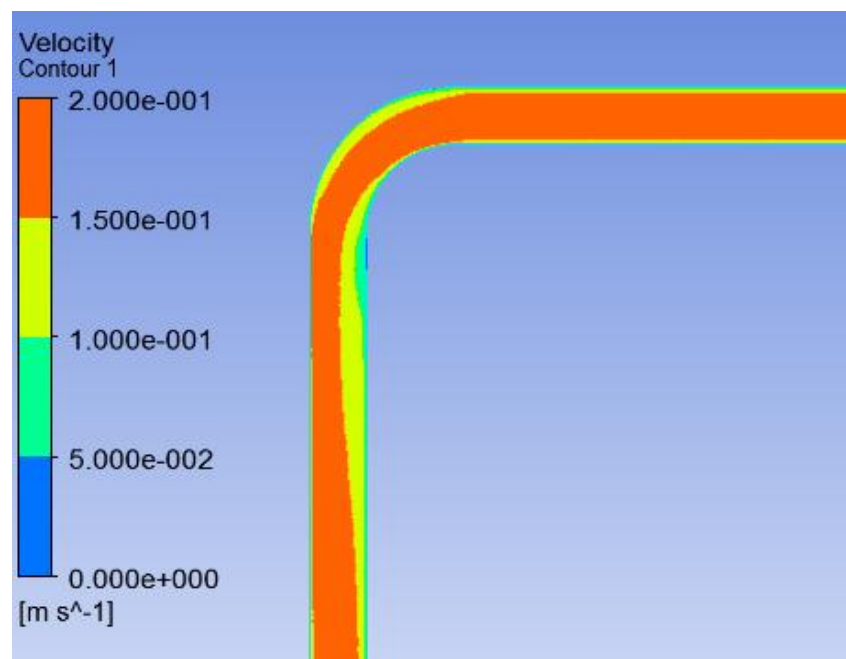


**Figure 4.17** The seawater velocity profile around type 2 of 90 degree bend.

This type can reduce the dead zones and make more uniform velocity than base model. However, it still has some dead zone after the fluid pass the bend as shown in Figure 4.17. Thus, the radius of curvature was increased for the next configuration.

Type 3: This type uses the radius curvature of 0.3 m

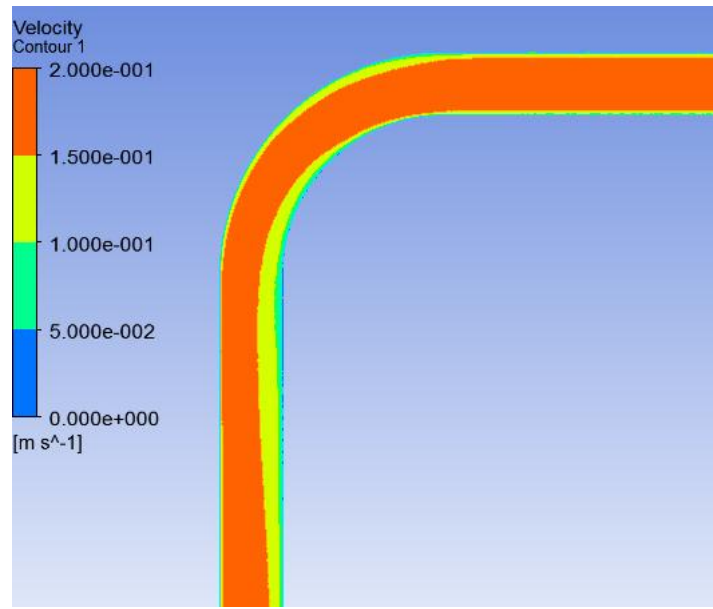


**Figure 4.18** The seawater velocity profile around type 3 of 90 degree bend.

This figure shows a small green and blue color zone which means this type can eliminate most of dead zone. Moreover, the velocity is more uniform than the base model so this type has a chance to be the optimal configuration of 90 degree bend.

Type 4: This type uses 2 angle of 45 degree connected by the straight pipe.

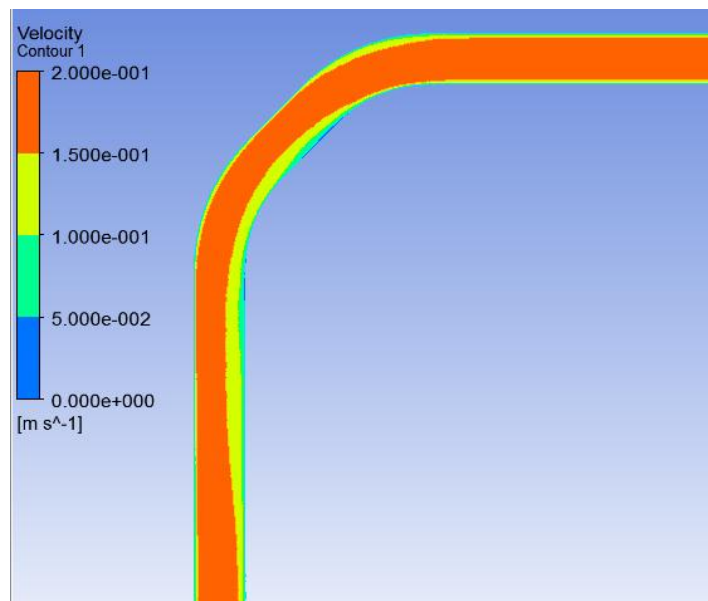


**Figure 4.19** The seawater velocity profile around type 4 of 90 degree bend.

The result of this type is similar to the result of type 3. It can eliminate almost all dead zones and give more uniform velocity.

The conclusion about the dead zone percentage of each type which calculates from histograms in Appendix B and the percentage of the dead zone reduction from the standard 90 degree bend are shown in Table 4.3.

**Table 4.3** Percentage of the dead zone of 90 degree bend

Type of 90 degree bend	%Dead zone	%Reduction
Standard	90.940	0.000
Type 1	91.192	-0.277
Type 2	90.920	0.022
Type 3	<b>71.689</b>	<b>21.168</b>
Type 4	77.799	14.450

Refer to Table 4.3, type 1 cannot reduce the dead zone from the base 90 degree bend and type 2 can decrease the dead zone only 0.022% but is not significant. Therefore, these two types of bend are neglected. On the other hand, types 3 and 4 are selected to calculate the pressure loss because they can reduce the higher pressure loss and make a uniform velocity.

#### 4.2.2.2 Comparison of pressure loss

The pressure loss is calculated from equation (4.1.3.2). Table 4.4 shows the pressure loss comparison between the standard type with the other types which the pressure loss is calculated at same length and the calculation method is shown in Appendix C.

**Table 4.4** Pressure loss of each case and percentage of the pressure loss reduction.

90 degree bend type	Ploss	delta Ploss	% Reduction
Standard	6.569	0.000	0.000
Type 3	<b>5.790</b>	<b>0.779</b>	<b>11.863</b>
Type 4	6.470	0.099	1.503

As Table 4.4, type 3 and type 4 can reduce the pressure loss from base case by 11.863% and 1.503%, respectively. Therefore, type 3 is the optimal configuration of 90 degree bend since it has the highest percentage of the dead zone reduction and the pressure loss reduction. In addition, it can make more uniform velocity also.

One can conclude that the optimal configuration of U-bend is type 5 which uses the radius of curvature 0.35 m and the angle of arc 210 degree. The optimal configuration of 90 degree bend is type 3 with the radius at 0.3 m.

### 4.3 Optimal of the tubular photobioreactor model

The optimal tubular photobioreactor model which replacing the standard U-bend and 90 degree bend with the optimal configuration of U-bend and 90 degree bend was simulated in order to find the optimal air inlet velocity. The relationship between the air inlet velocity and seawater velocity is shown in Figure 4.20.

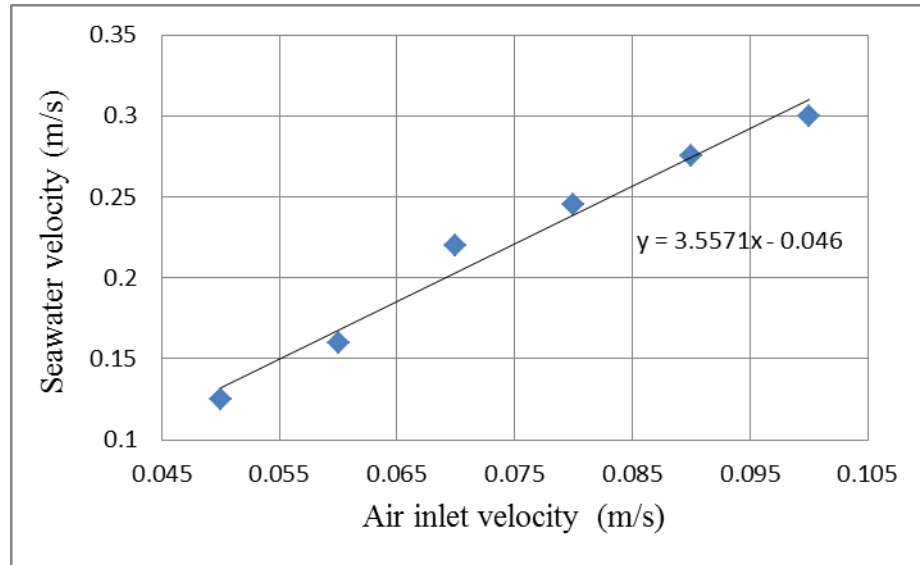


**Figure 4.20** The relationship between air inlet velocity and seawater velocity

From the relationship of these two velocities, the optimal air inlet velocity that can make the seawater velocity at 0.17 m/s is 0.061 m/s. It is less than the air inlet velocity used in the basic tubular photobioreactor (0.072 m/s as shown in section 4.1.1). The comparison of air inlet velocity used in the basic tubular photobioreactor and in the optimal tubular photobioreactor is shown in Figure 4.21.

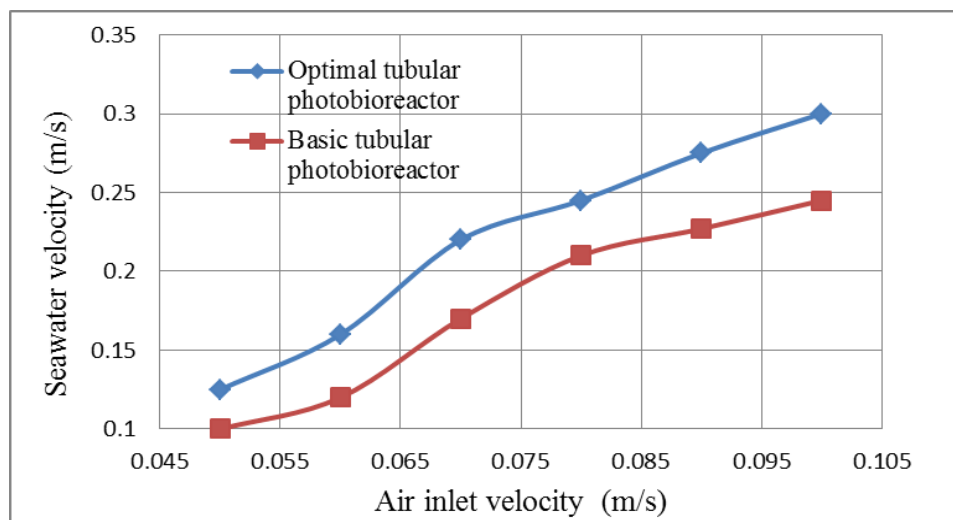


**Figure 4.21** The comparison of air inlet velocity that used in the basic tubular photobioreactor and the optimal tubular

At the same seawater velocity, the air inlet velocity in the optimal tubular photobioreactor as shown in blue line is less than the air inlet velocity in the basic tubular photobioreactor as shown in red line. Since the pressure loss of the optimal configuration decreases so the air inlet velocity that uses to push the seawater decreases too. This is one of advantages of designing the optimal configuration because the system will use the less energy to input the air into the reactor at the same required seawater velocity. The relationship between air inlet velocity and energy input due to aeration [7] is shown in equation 4.3.1 and Figure 4.22

$$P_G = Q_G h_r g \rho \quad (4.3.1)$$

Where  $P_G$  is the energy input due to aeration (J/s),  $Q_G$  is the volumetric flow rate of gas ( $\text{m}^3/\text{s}$ ),  $h_r$  is height of riser (m),  $g$  is acceleration of gravity ( $\text{m}/\text{s}^2$ ) and  $\rho$  is density of the seawater ( $\text{kg}/\text{m}^3$ )

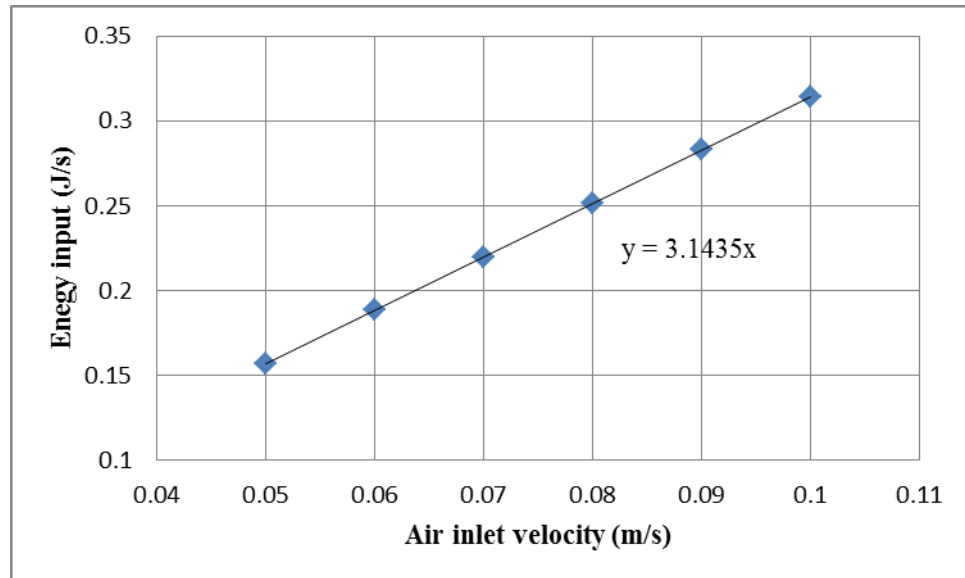


**Figure 4.22** The relationship between air inlet velocity and energy input

Figure 4.22 shows the energy input due to the aeration will increase when the air inlet velocity increase. At the seawater velocity 0.17 m/s, the basic tubular photobioreactor requires energy input 0.226 J/s (at air inlet velocity 0.072 m/s) while the optimal tubular photobioreactor requires energy input 0.192 J/s (at air inlet velocity 0.061 m/s). Thus, the optimal tubular photobioreactor can reduce the energy input equal to 15.04%.

## **CHAPTER 5 CONCLUSION AND RECCOMENDATION**

### **5.1 Conclusion**

The objective of this thesis is to modify the basic tubular photobioreactor in order to minimize the dead zones, make more uniform velocity and reduce the pressure loss. The simulation result of the basic tubular photobioreactor shows the dead zone around the standard U-bend and 90 degree bend. Thus, the new bend configurations were designed to solve this problem. There are 6 configurations of U-bend and 4 configurations of 90 degree bend which were proposed in this research. The result shows the optimal configuration of U-bend is type 5 which has the radius of curvature 0.35 m and the angle of arc 210 degree and the optimal configuration of 90 degree bend is type 3 of 90 degree bend which has the radius of curvature 0.3 m. Since both of them can eliminate the dead zone significantly, generate more uniform velocity than the base model and reduce the pressure loss. The optimal U-bend can reduce the dead zone from the standard U-bend 9.459% and the pressure loss 12.534%. The optimal 90 degree bend can reduce the dead zone from the standard 90 degree bend 21.618 % and the pressure loss 11.863%.

This thesis is also to find the optimal air inlet velocity that makes the seawater velocity equal to 0.17 m/s. The optimal air inlet velocity of the basic tubular photobioreactor model is 0.072 m/s and the optimal air inlet velocity of the optimal tubular photobioreactor model is 0.061m/s. The less air inlet velocity requirement of the optimal tubular photobioreactor can reduce the energy input due to aeration 15.04%.

### **5.2 Recommendation**

- Use the high performance computer to simulate the model because the actual tubular photobioreactor is very large. The personal computer ability cannot generate the fine mesh and use a lot of time to solve the solution.
- Increase the length of pipe and rearrange the pipe to minimize the land demand as the multiple U-bend tubular photobioreactor.
- Add the solid phase that represents the algae and the growth model to study the parameters that affect to the algae and predict the yield of product.

## REFERENCES

- [1] W.H. Adey, Maria Faust Mark M. Littler. **Algae Research** [online]. Available: <http://botany.si.edu/projects/algae/index.htm>, [3 May 2011].
- [2] **League of Women Voter of New Jersey Education Fund** [online]. Available: [http://www.lwvnj.org/alternativeenergy/biomass\\_microalgae.pdf](http://www.lwvnj.org/alternativeenergy/biomass_microalgae.pdf), [3 May 2011]
- [3] Ling Xu, Pamela J. Weathers, Xue-Rong Xiong, Chun-Zhao Liu. 2009. Microalgal bioreactors: Challenges and opportunities. **Engineering in Life Science**: 178-189
- [4] C.U. Ugwu, H. Aoyagi, H. Uchiyama, 2008. Photobioreactors for mass cultivation of algae, **Bioresource Technology**, 99, 4021–4028
- [5] J. Doucha, K. Livansky, K. Kostelnik, 1996. Thin-layer microalgal culture technology. **Abstracts of the 7th Int. Conf. of Appl. Algology**, Knysna, South Africa, 32.
- [6] E. Molina, J. Fernandez, F.G. Acien, Y. Chisti, 2001. Tubular photobioreactor design for algal cultures. **Journal of Biotechnology**. 92, 113-131
- [7] F.G. Acien Fernandez, J.M. Fernandez, Sevilla, J.A. Sanchez Perez, E. Molina Grima, Y. Chisti., 2001. Airlift-driven external-loop tubular photobioreactors for outdoor production of microalgae: assessment of design and performance. **Chemical Engineering Science**. 56, 2721-2732
- [8] E. Molina, F. G. Fernandez, F. G. Camacho, F. C. Rubio, Y. Chisti., 2000. Scale-up of tubular photobioreactors. **Journal of Appl. Phycol.** 12, 355–368.
- [9] Y. Chisti., 1989. *Airlift Bioreactors*. Elsevier, London.
- [10] Y. Chisti., 1999a. Shear sensitivity. In: Flickinger, M.C., Drew, S.W. (Eds.), *Encyclopedia of Bioprocess Technology: Fermentation, Biocatalysis and Bioseparation*, vol.5. Wiley, New York, pp. 2379–2406.
- [11] F. Camacho Rubio, F.G. Acien Fernandez, J.A. Sanchez Perez, F. Garcia Camacho, E. Molina Grima, 1999. Prediction of dissolved oxygen and carbon dioxide concentration profiles in tubular photobioreactors for microalgal culture. **Biotechnol. Bioeng.** 62, 71–86.
- [12] J.P. Bitog, I.-B. Lee, C.-G. Lee, K.-S. Kim, H.-S. Hwang, S.-W. Hong, I.-H. Seo, K.-S. Kwon, E. Mostafa., 2011. Application of computational fluid dynamics for modeling and designing photobioreactors for microalgae production: A review. **Journal of Computer and Electronics in Agriculture**, pp. 2379–2406.
- [13] A.R. Kommareddy, G.A. Anderson, 2005. Mechanistic Modeling of Photobioreactor System. **ASAE Paper No. 057007**. ASAE, St. Joseph, Michigan

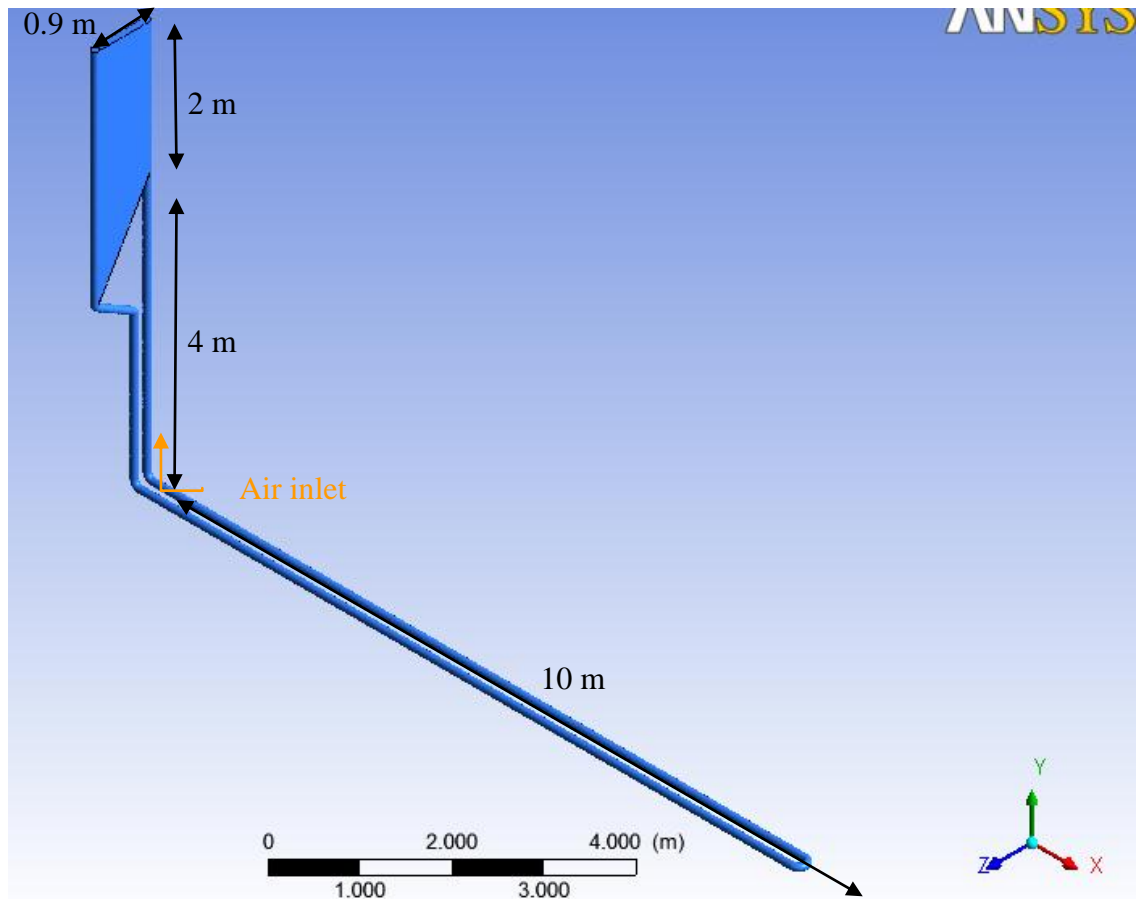
- [14] A.P. Carvalho, L.A. Meireles, F.X. Malcata, 2006. Microalgal reactors: a review of enclosed system designs and performances. **Biotechnology Progress** 22,1490–1506.
- [15] C. Guin, D. Chaumont, 1991. Cell fragility-key problem of microalgae mass production on closed photobioreactors. **Bioresource Technology** 38, 145–151.
- [16] **The Bernoulli Equation for an Incompressible, Steady Fluid Flow** [Online], Available: [http://www.4physics.com/phy\\_demo/bernoulli-effect-equation.html](http://www.4physics.com/phy_demo/bernoulli-effect-equation.html), [15 May 2011].
- [17] B. Bird, W. E. Stewart, & E. N. Lightfoot, 1960. **Transport phenomena**. New York: John Wiley & Sons.
- [18] J.C. Merchuk, M. Gluz, , I. Mukmenev, 2000. Comparison of photobioreactors for cultivation of the red Porphyridium sp. **Journal of Chemical Technology and Biotechnology** 75, 1119–1126.
- [19] J. Gimbut, 2009. Assessment of the turbulence models for modeling of bubble column. **The Institution of Engineers Journal**, Malaysia 70 (4).
- [20] B.E. Launder, D.B. Spalding, 1972. **Lecture on Mathematical Models of Turbulence**. Academic Press, London.
- [21] J.B. Joshi, 2001. Computational flow modelling and design of bubble column reactors. *Chemical Engineering Science* 56, 5893–5933.
- [22] **Modeling Turbulence. ANSYS FLUENT User's Guide 2010, Chapter13**, [Online], Available: <http://www.ansys.com>, [15 May 2011].

## **APPENDIX A**

### **Tubular photobioreactor configuration**

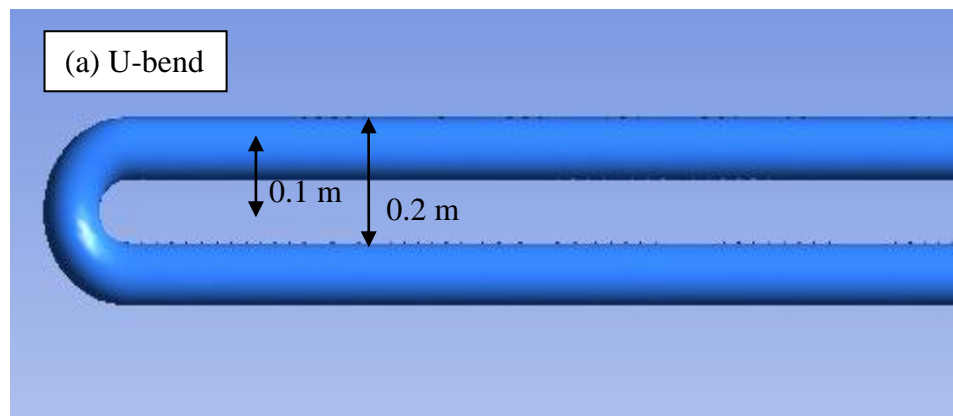
## A.1 The basic tubular photobioreactor

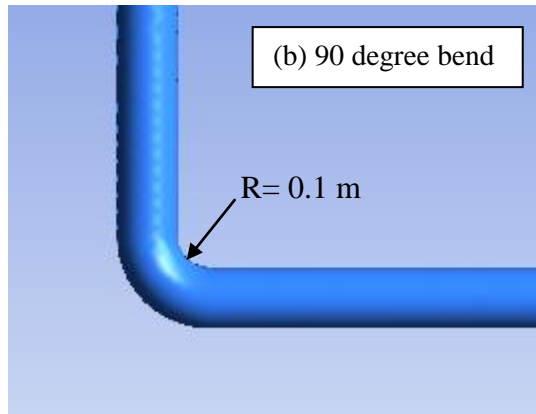
The provided configuration of the basic tubular photobioreactor is shown in Figure A.1.



**Figure A.1** Basic tubular photobioreactor

As Figure A.1, the height and width of the gas-liquid separator is 2 m and 0.9 m respectively and the height of the riser is 4 m. The length of straight pipe of solar collector tube is 10 m and the diameter of the tube is 0.1 m. Moreover, it shows the position of air inlet.





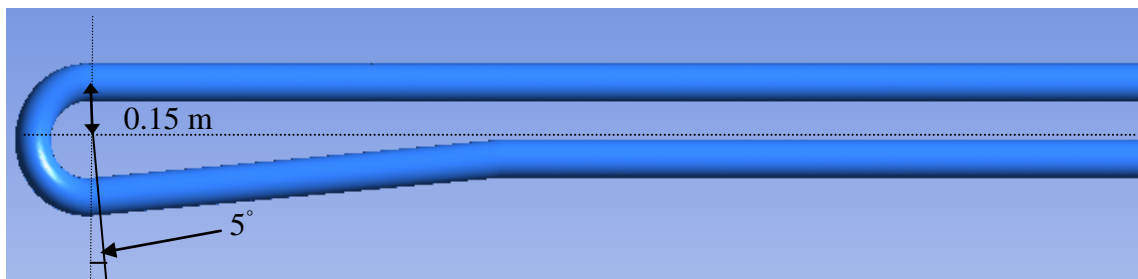
**Figure A.2** Bend of the basic tubular photobioreactor (a) U-bend, (b) 90 degree bend

Figure A.2 (a) shows the distance between the walls of tube is 0.2 m and the radius of U-bend is 0.1 m. The radius of the 90 degree bend is 0.1 m as shown in Figure A.2 (b)

### A.2 Adapted U-bend configuration

The dimension of the U-bend configuration of each type is shown below.

Type 1: The radius of U-bend is 0.15 m and the return angle to the straight pipe is 5 degree



**Figure A.3** Type 1 of U-bend configuration

Type 2: The radius of U-bend is 0.5 m and the return angle to the straight pipe is 5 degree

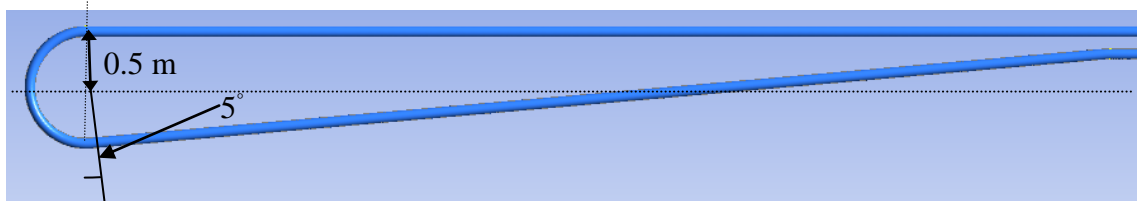


**Figure A.4** Type 2 of U-bend configuration

Type 3: The radius of U-bend is 0.5 m and the angle of arc is 225 degree

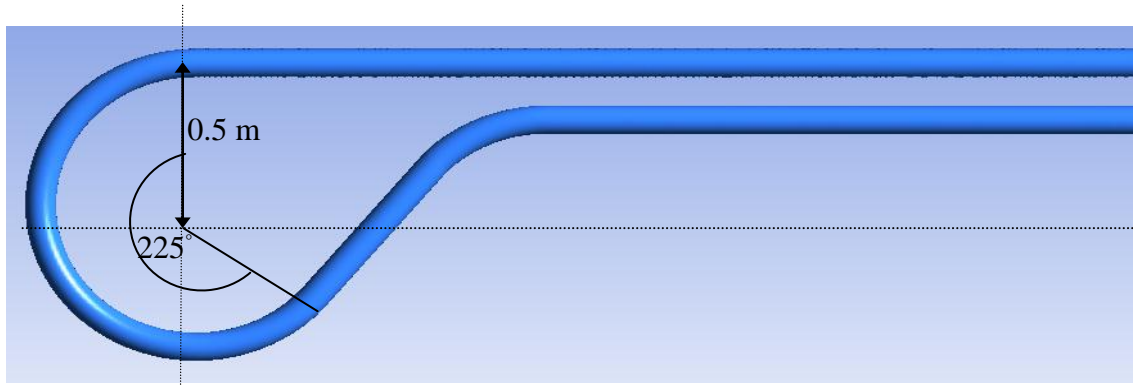


**Figure A.5** Type 3 of U-bend configuration

Type 4: The radius of U-bend is 0.35 m and the angle of arc is 225 degree



**Figure A.6** Type 4 of U-bend configuration

Type 5: The radius of U-bend is 0.35 m and the angle of arc is 210 degree

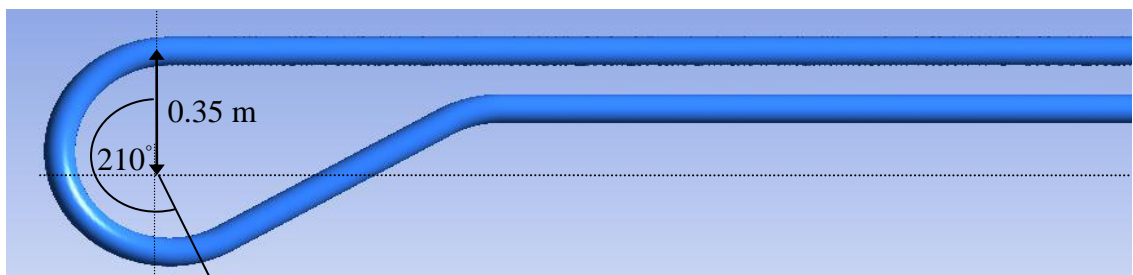


**Figure A.7** Type 5 of U-bend configuration

Type 6: The radius of U-bend is 0.25 m and the angle of arc is 225 degree



**Figure A.8** Type 6 of U-bend configuration

### A.3 Adapted 90 degree bend configuration

The dimension of the 90 bend configuration of each type is shown below.

Type 1: The sharp 90 degree bend  
(radius = 0.05 m)

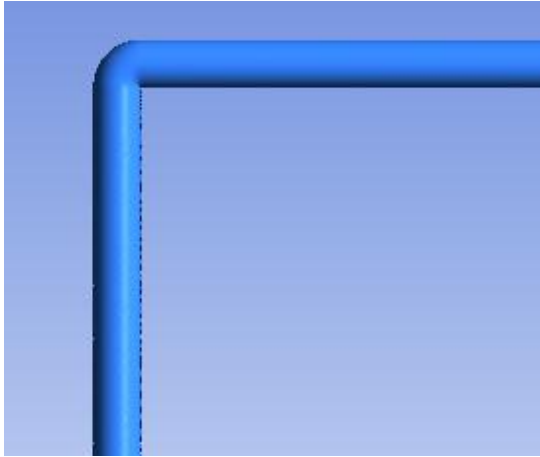


**Figure A.9** Type 1 of 90 degree bend configuration

Type 2: The radius curvature is 0.2 m

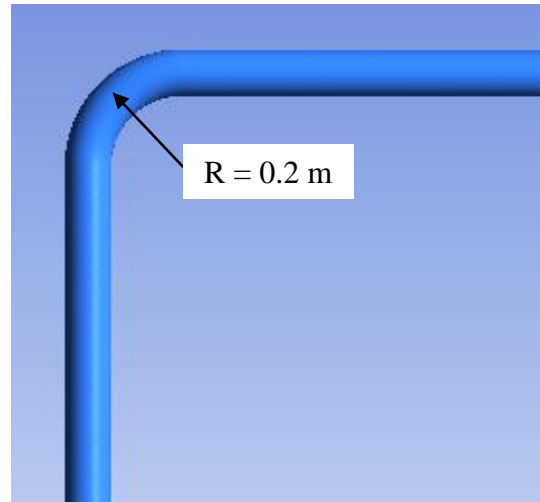


**Figure A.10** Type 2 of 90 degree bend configuration

Type 3: The radius curvature is 0.3 m

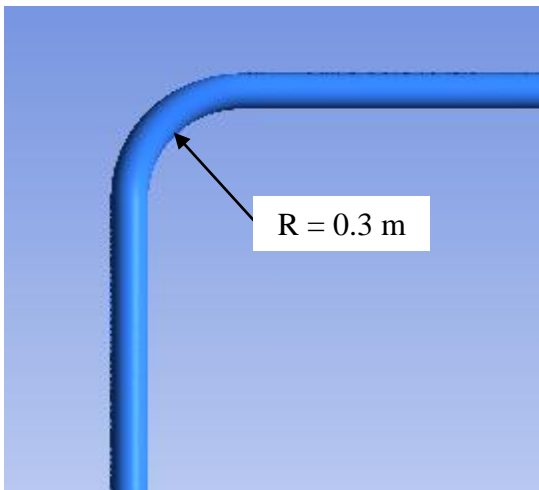


**Figure A.11** Type 3 of 90 degree bend configuration

Type 4: This type use 2 angle of 45 degree connected by the straight pipe.

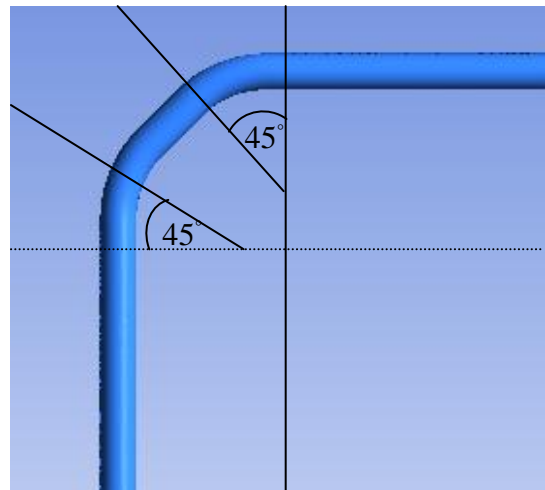


**Figure A.12** Type 4 of 90 degree bend configuration

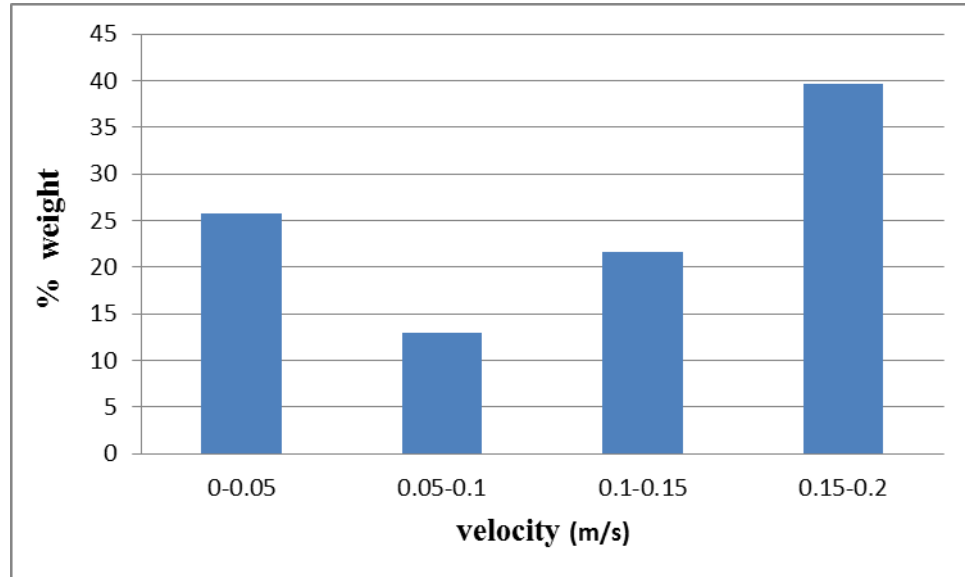
## **APPENDIX B**

Histogram of velocity

## B.1 Dead zone histograms of each U-bend type

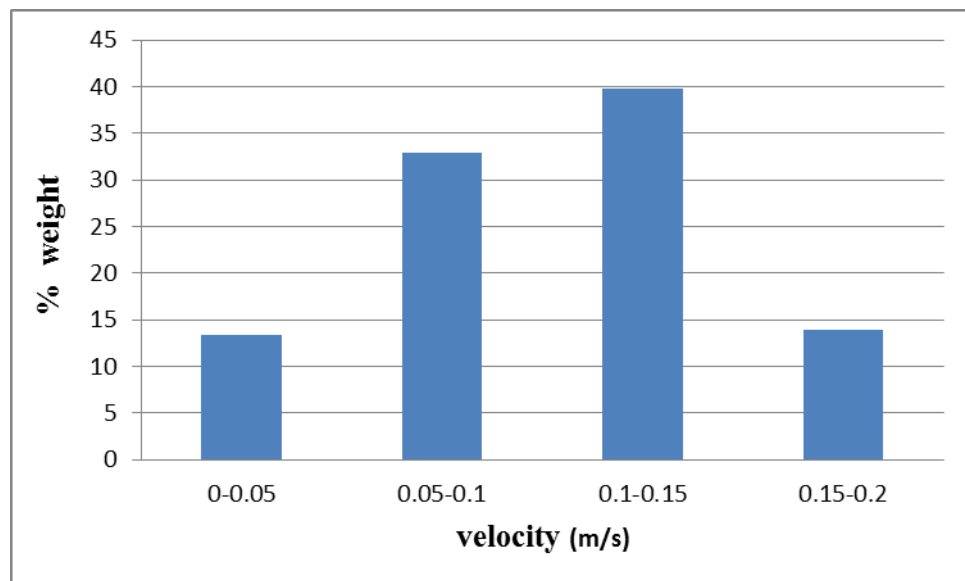
The histogram shows the percentage by weight of sea water in the different velocity ranges.

### Type 1

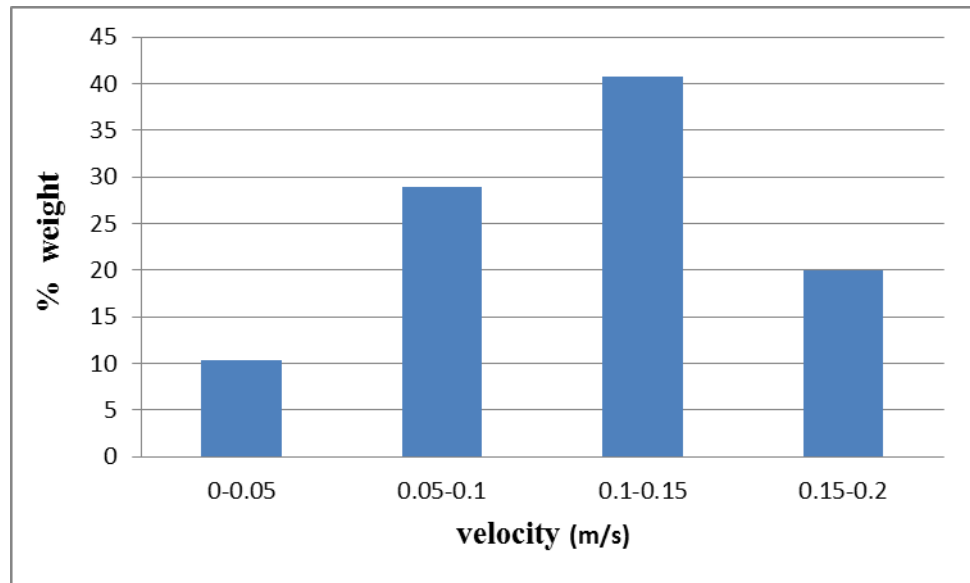


**Figure B.1** The percentage by weight of fluid in the different velocity ranges of type 1 of U-bend

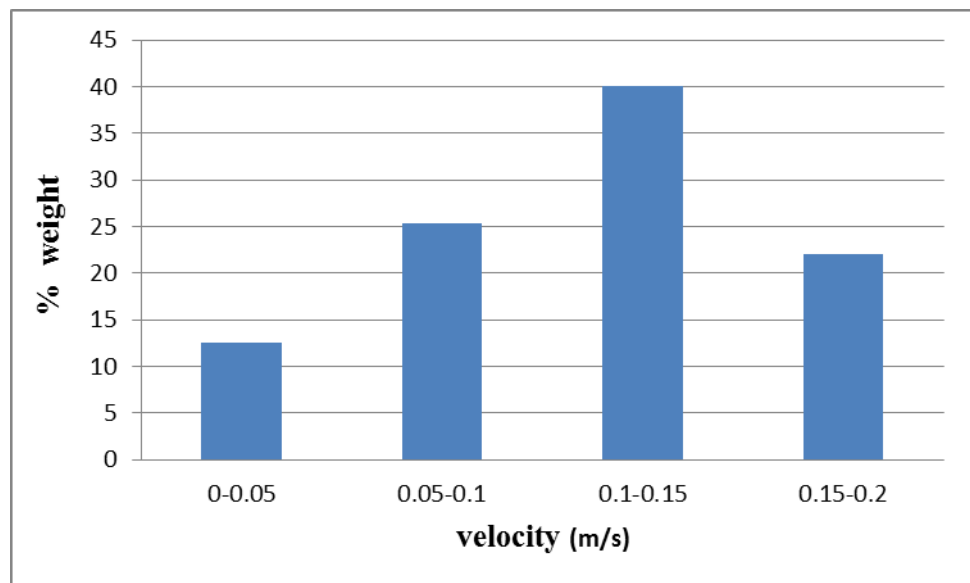
### Type 3



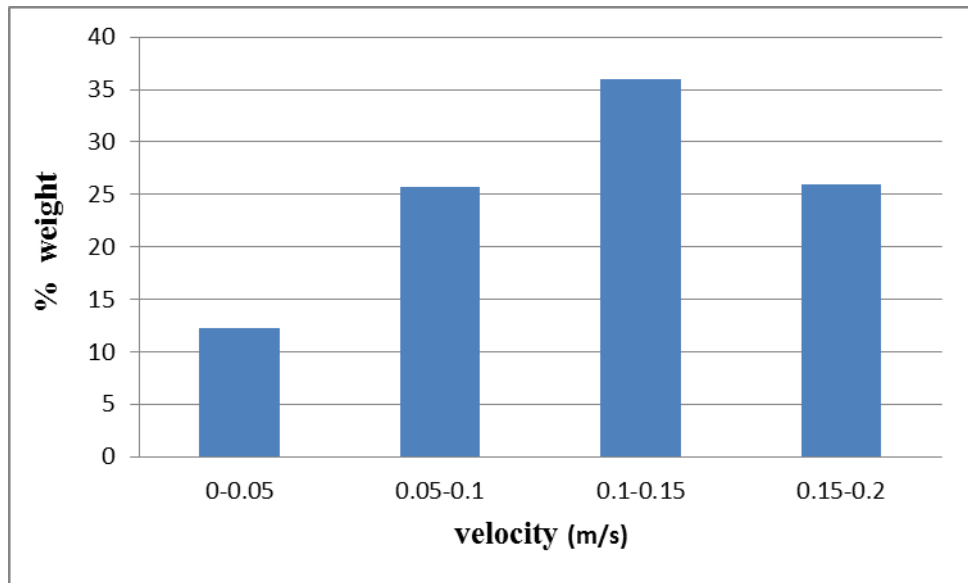
**Figure B.2** The percentage by weight of fluid in the different velocity ranges of type 3 of U-bend

Type 4

**Figure B.3** The percentage by weight of fluid in the different velocity ranges of type 4 of U-bend

Type 5

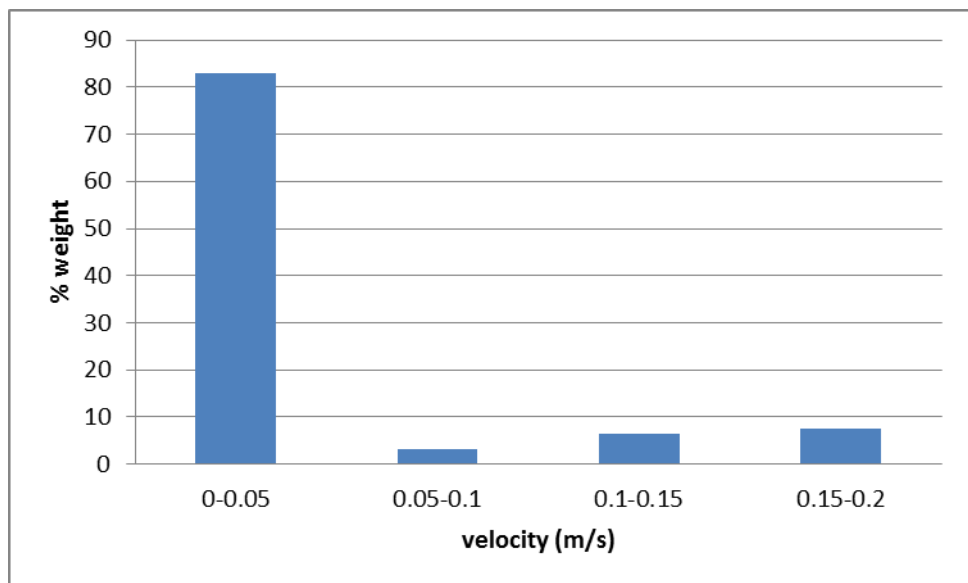
**Figure B.4** The percentage by weight of fluid in the different velocity ranges of type 5 of U-bend

Type 6

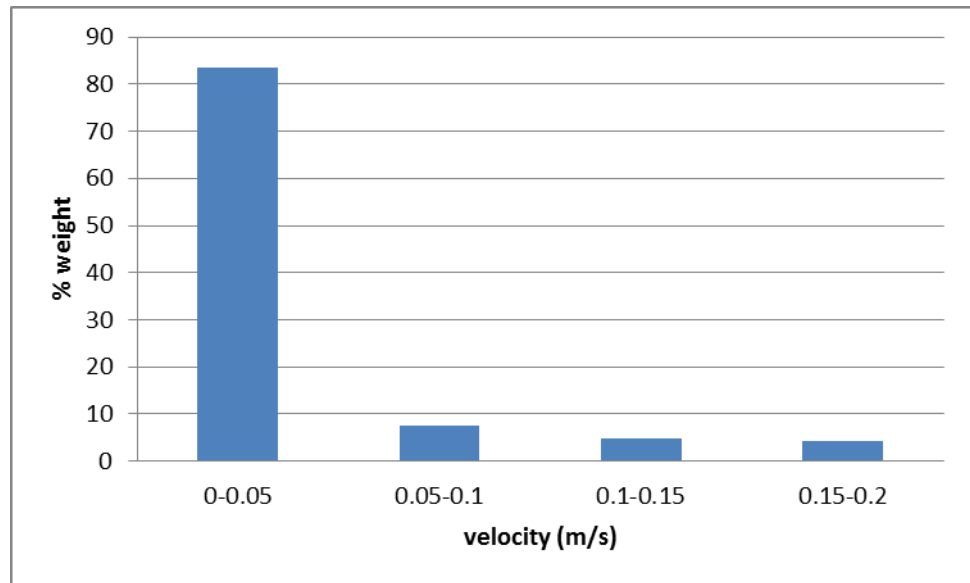
**Figure B.5** The percentage by weight of fluid in the different velocity ranges of type 6 of U-bend

## B.2 Dead zone histograms of each 90 degree bend type

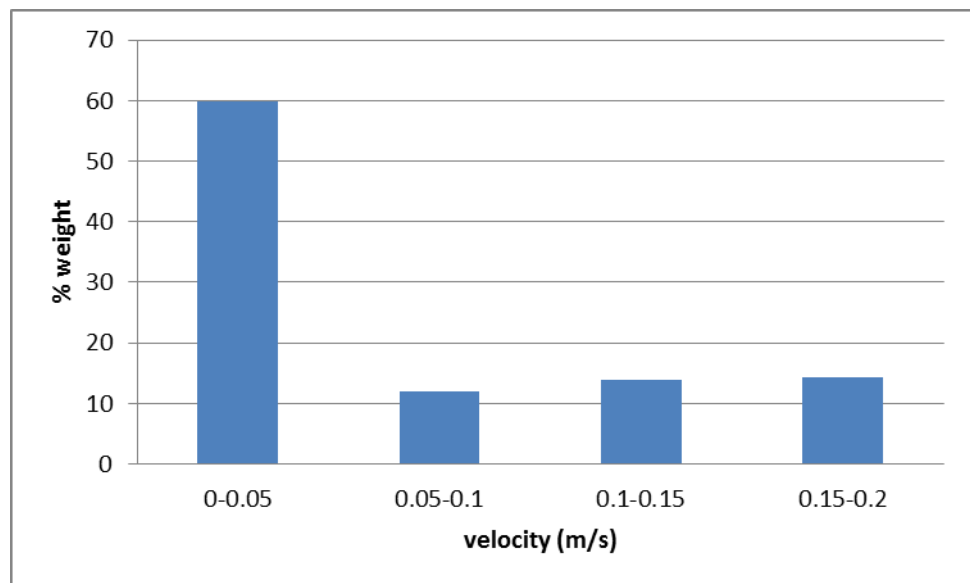
The histogram shows the percentage by weight of sea water in the different velocity ranges.

Type 1

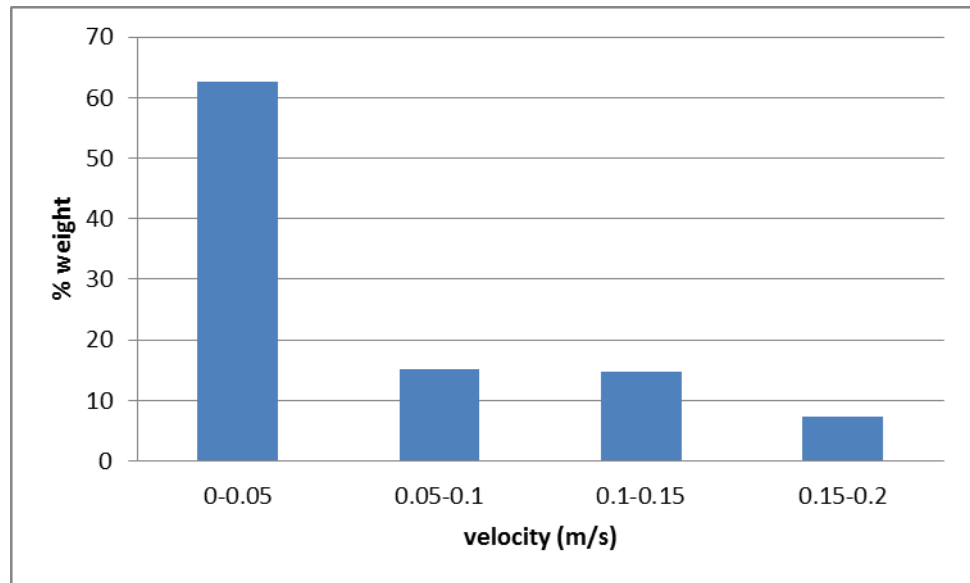
**Figure B.6** The percentage by weight of fluid in the different velocity ranges of type 1 of 90 degree bend

Type 2

**Figure B.7** The percentage by weight of fluid in the different velocity ranges of type 2 of 90 degree bend

Type 3

**Figure B.8** The percentage by weight of fluid in the different velocity ranges of type 3 of 90 degree bend

Type 4

**Figure B.9** The percentage by weight of fluid in the different velocity ranges of type 1 of 90 degree bend

## **APPENDIX C**

### **Pressure loss calculation**

**Table C.1** Pressure loss calculation of U-bend

U-bend	Standard		Type 1		Type 3		Type 4		Type 5		Type 6	
Sampling	Point 1	Point 2	Point 1	Point 2	Point 1	Point 2	Point 1	Point 2	Point 1	Point 2	Point 1	Point 2
- Velocity, m/s	0.160	0.157	0.158	0.157	0.158	0.148	0.157	0.157	0.157	0.157	0.158	0.157
- Pressure, Pa	27.884	10.457	27.577	11.271	33.863	18.406	31.551	15.211	30.773	15.150	30.333	13.740
Pressure loss, Pa												
- Kinetic term	13.128	12.635	12.779	12.573	12.656	11.177	12.580	12.645	12.571	12.519	12.702	12.536
- Fluid pressure	27.884	10.457	27.577	11.271	33.863	18.406	31.551	15.211	30.773	15.150	30.333	13.740
Total, Pa	41.012	23.092	40.356	23.844	46.519	29.582	44.131	27.856	43.343	27.669	43.035	26.276
Ploss, Pa		17.920		16.511		16.937		16.275		15.674		16.759

**Table C.2** Pressure loss calculation of 90 degree bend

90 degree bend	Std_90-bend		Type 1		Type 2		Type 3	
Sampling	Point 1	Point 2	Point 1	Point 2	Point 1	Point 2	Point 1	Point 2
- Velocity	0.160	0.150	0.158	0.148	0.157	0.151	0.158	0.140
- Pressure	12.061	7.120	12.025	7.874	12.262	7.403	13.254	9.505
Pressure loss								
- Kinetic term	13.112	11.484	12.692	11.189	12.590	11.660	12.679	9.958
- Fluid pressure	12.061	7.120	12.025	7.874	12.262	7.403	13.254	9.505
Total	25.173	18.604	24.717	19.064	24.852	19.063	25.933	19.463
Ploss		6.569		5.653		5.790		6.470

Table B.1 and Table B.2 shows the pressure loss calculation of U-bend and 90 degree bend of each type. The example of calculation is shown below.

Example Pressure loss calculation of type 5 of U-bend

From the equation (4.1.3.1)

$$\rho g h_1 + \frac{\rho v_1^2}{2} + P_1 = \rho g h_2 + \frac{\rho v_2^2}{2} + P_2 + P_{loss} \quad (4.1.3.1)$$

$$h_1 = h_2, \quad \frac{\rho v_1^2}{2} + P_1 = \frac{\rho v_2^2}{2} + P_2 + P_{loss} \quad (4.1.3.2)$$

$$\frac{1020 \times 0.157^2}{2} + 30.773 = \frac{1020 \times 0.157^2}{2} + 15.150 + P_{loss}$$

$$P_{loss} = 15.674 \text{ Pa}$$

## **APPENDIX D**

Program set up

## Step 1: Loading mesh file

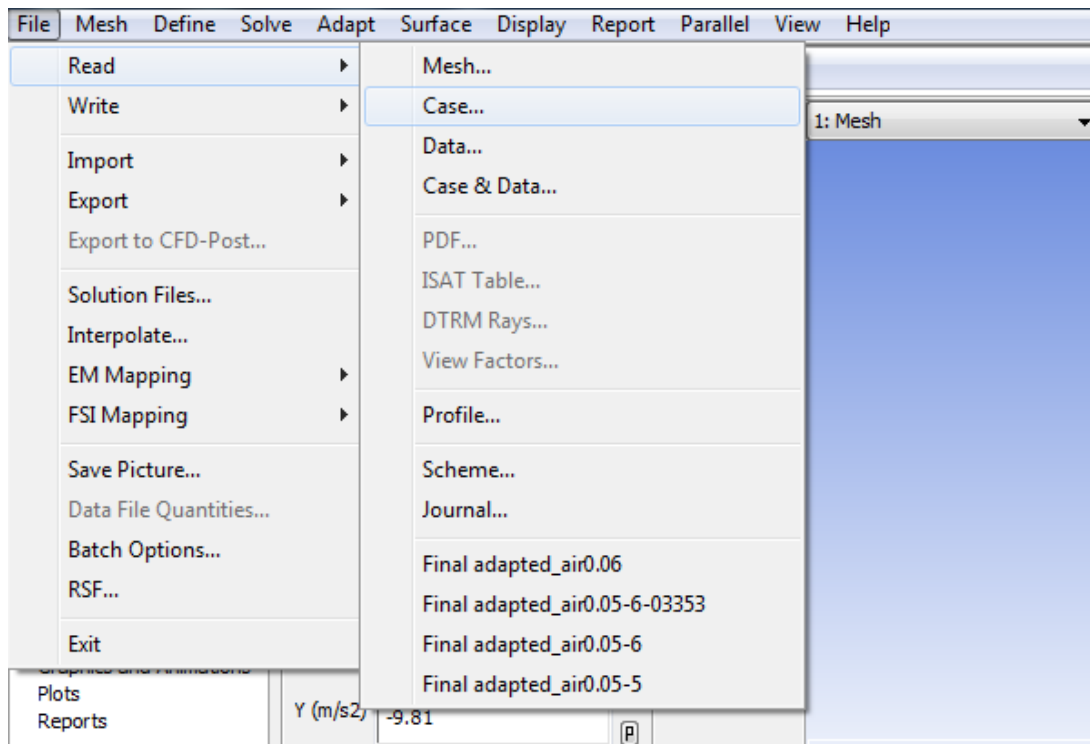


Figure D.1 Loading file method

## Step 2: Set up model

2.1 Enable Eulerian multiphase model. Define → Models → Multiphase

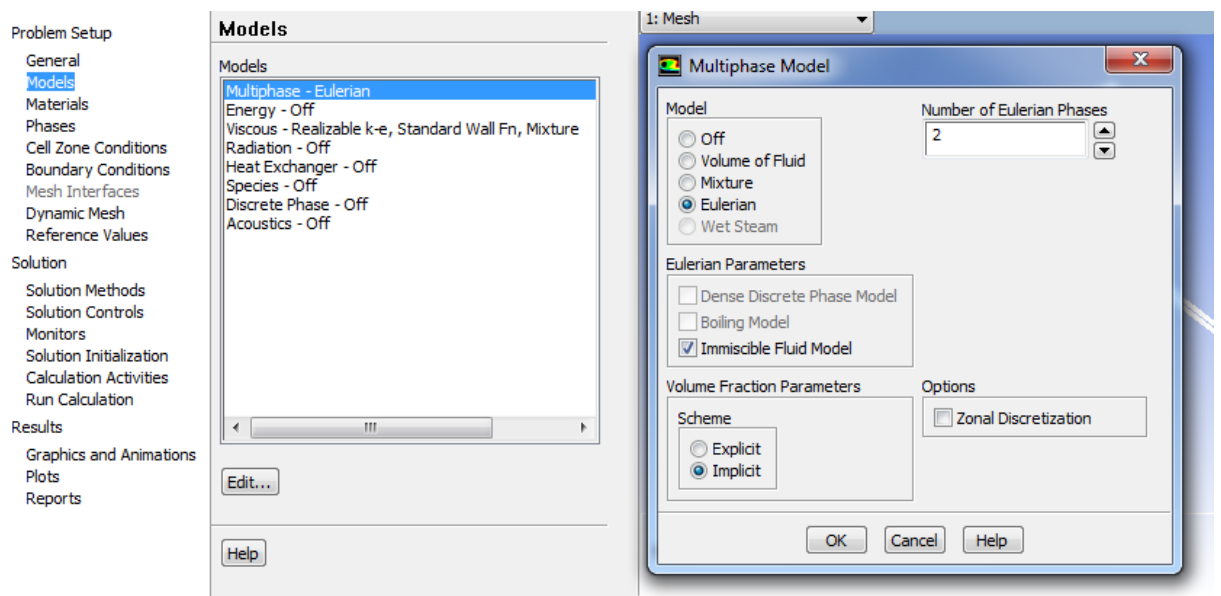


Figure D.2 Specify multiphase model method

## 2.2 Enable k-epsilon viscous model

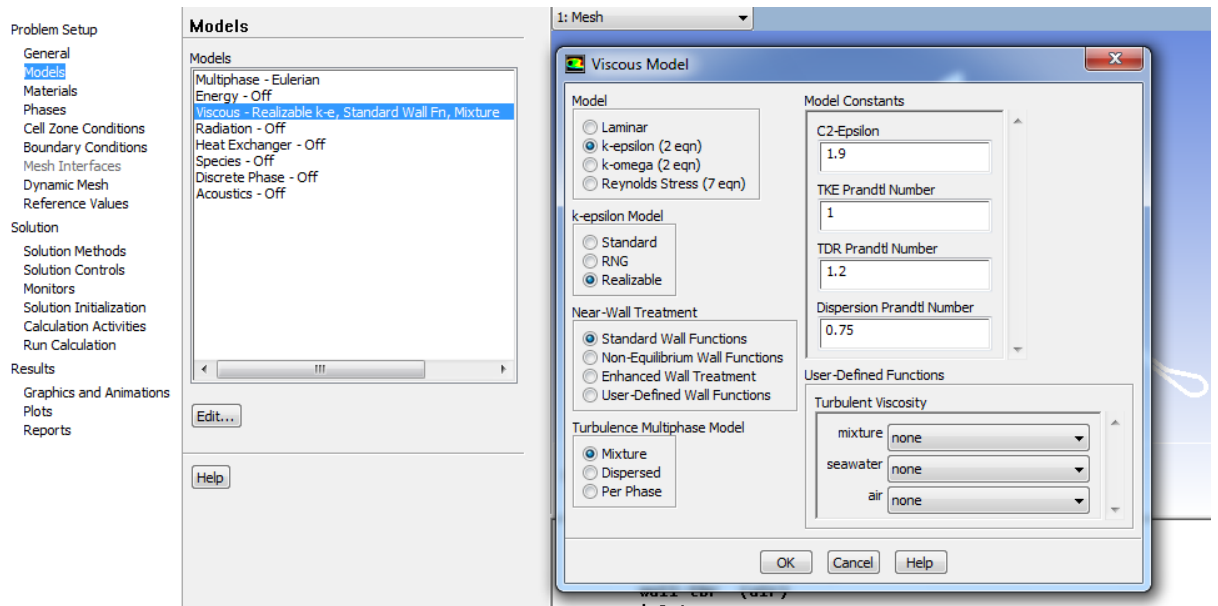


Figure D.3 Specify viscous model method

### Step 3: Add materials

Define → Material → Create/Edit

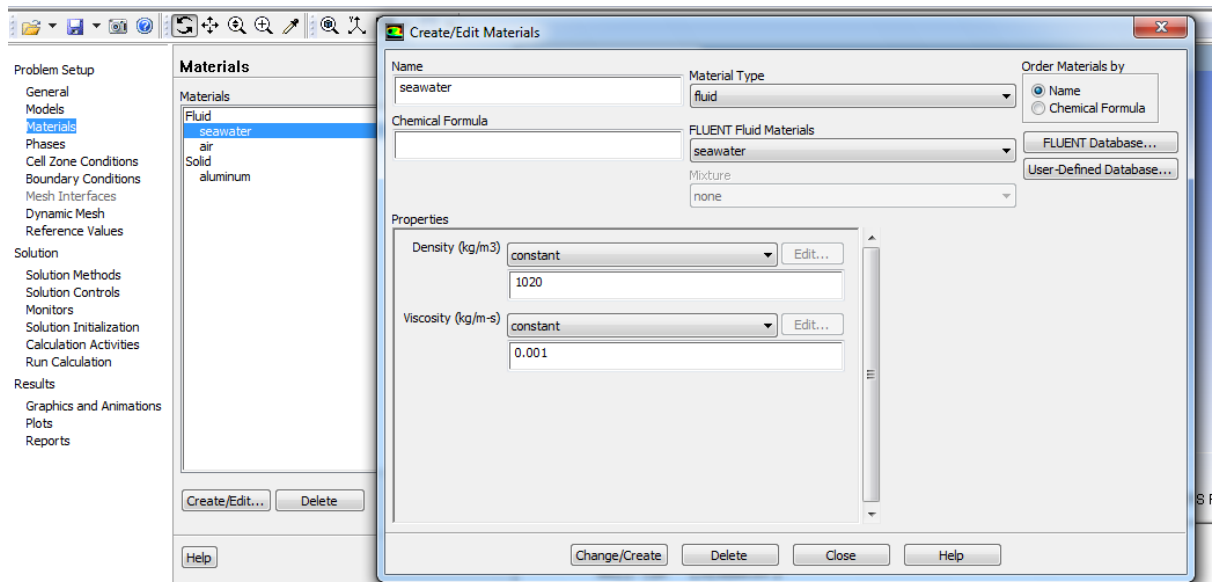


Figure D.4 Create material method

The materials that use in this model are seawater and air. Air is already has in the Fluent database. Seawater have to create by specify the density and viscosity which are 1020 kg/m<sup>3</sup> and 0.001 kg/(ms) respectively

## Step 4: Phase

Set seawater as the primary phase and air as the secondary phase

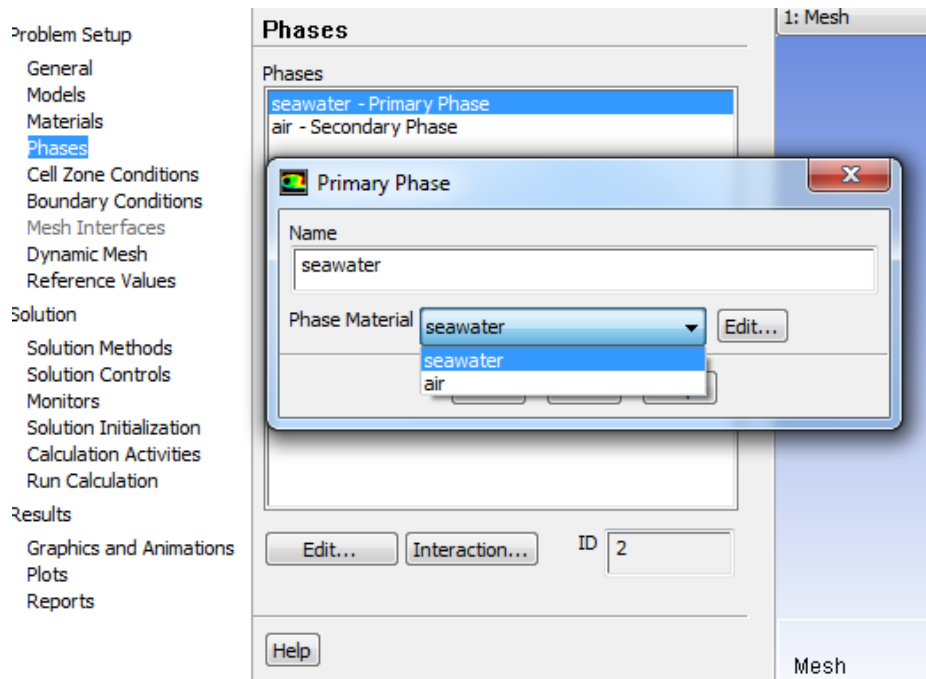


Figure D.5 Phase set up method

## Step 5: Boundary condition

Define → Boundary condition

### 5.1 Inlet Boundary condition

- Type of inlet is the velocity inlet.

#### 5.1.1 Phase → Mixture → Edit

- Select the specification method as intensity and hydraulic diameter.
- Specify the turbulent intensity is 5% and hydraulic diameter 0.01 m.

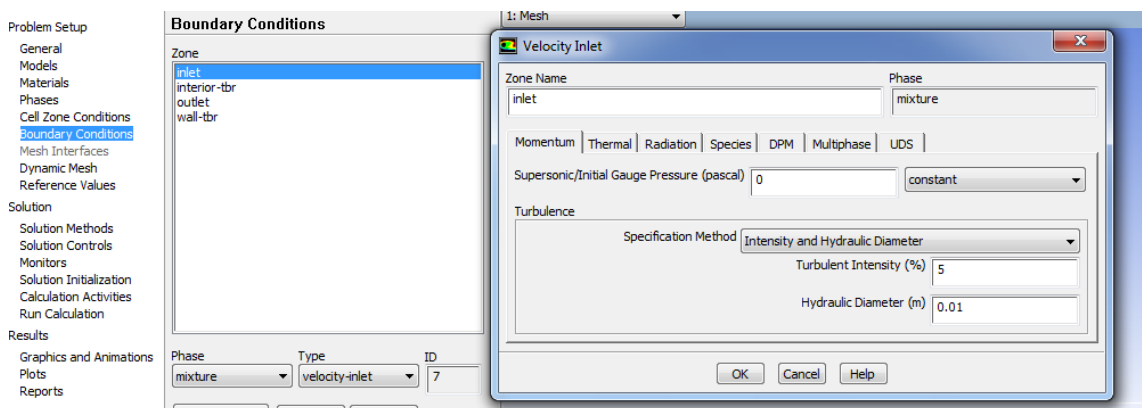
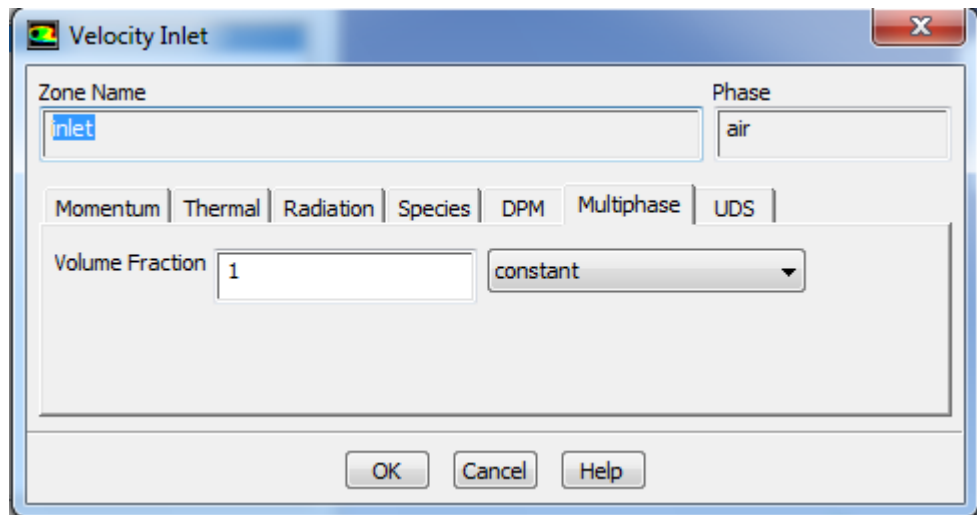
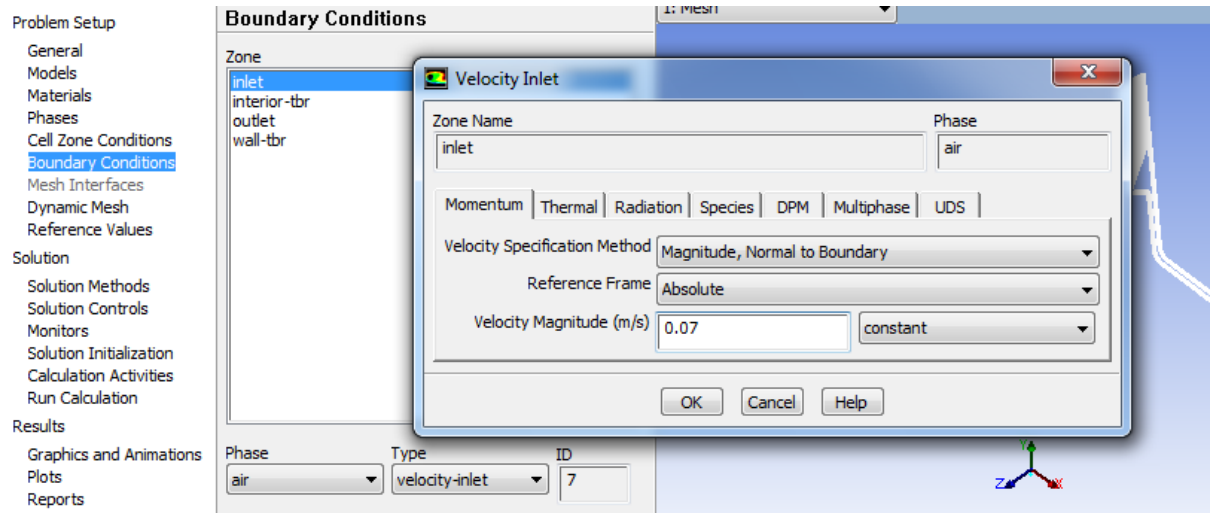


Figure D.6 Inlet boundary condition of mixture set up method

### 5.1.2 Phase → Air → Edit

- Specify the velocity inlet as 0.07 m/s (This value may be change following the cases)
- Click multiphase and specify the volume fraction of air is 1. (Only air feed into the system)



**Figure D.7** Inlet boundary condition of air set up method

## 5.2 Outlet Boundary condition

- Type of outlet is pressure outlet

### 5.2.1 Phase → Mixture → Edit

- Select the specification method as intensity and hydraulic diameter.
- Specify the turbulent intensity is 5% and hydraulic diameter 0.1 m.

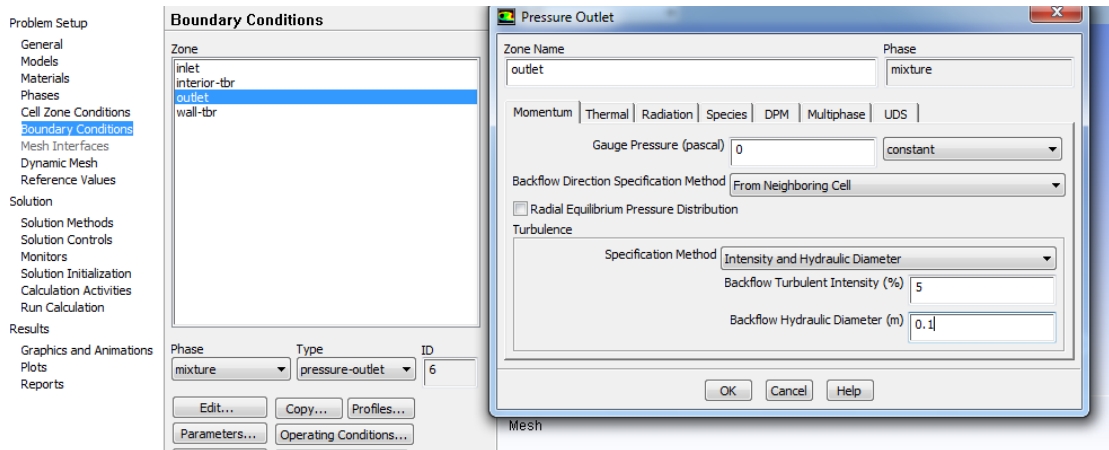


**Figure D.8** Outlet boundary condition of mixture set up method

### 5.2.2 Phase → Air → Edit

- Click multiphase and specify the backflow volume fraction of air is 1. (Only air can flow back into the system)

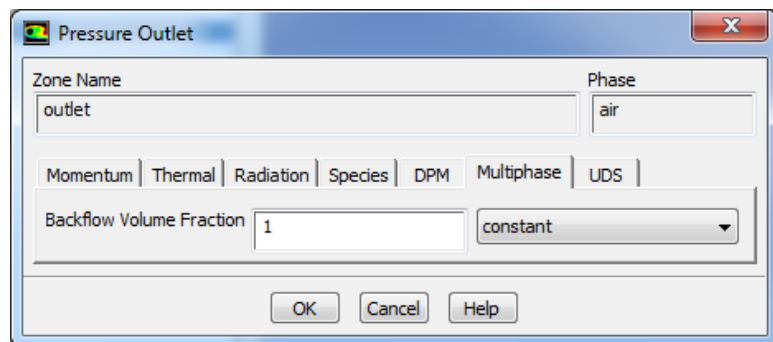


**Figure D.9** Outlet boundary condition of air set up method

### Step 6: Operating condition

Define → Operating condition → Enable the gravity (- 9.81m/s)

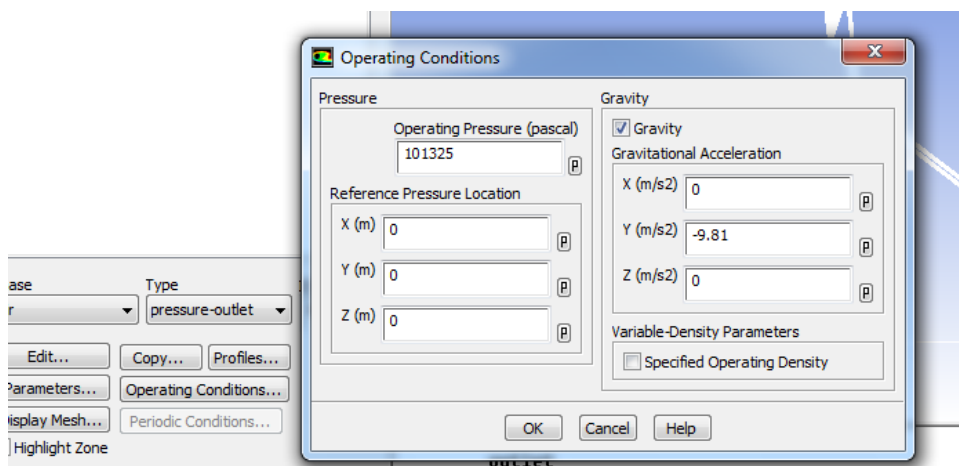


**Figure D.10** Operating condition set up method

## Step 7: Set the seawater level

Adapt → Region

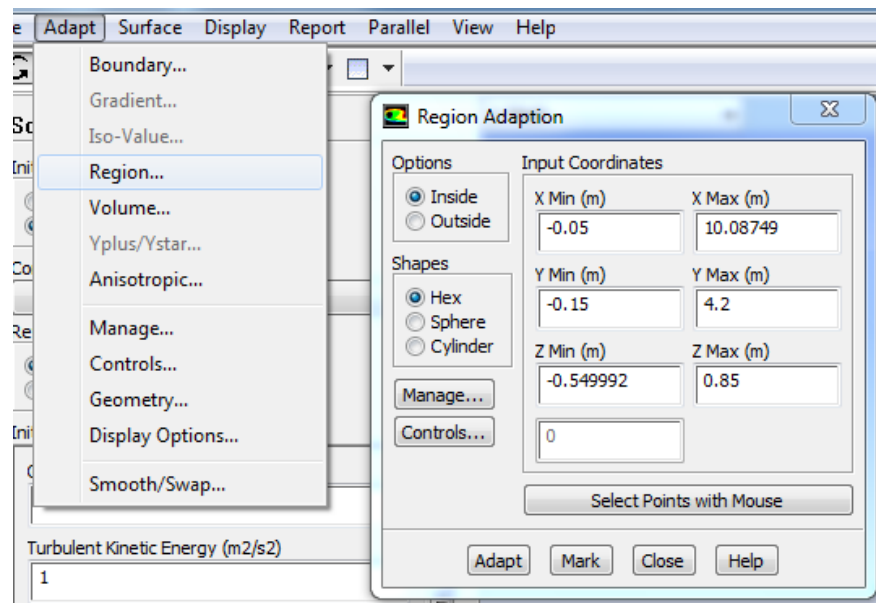
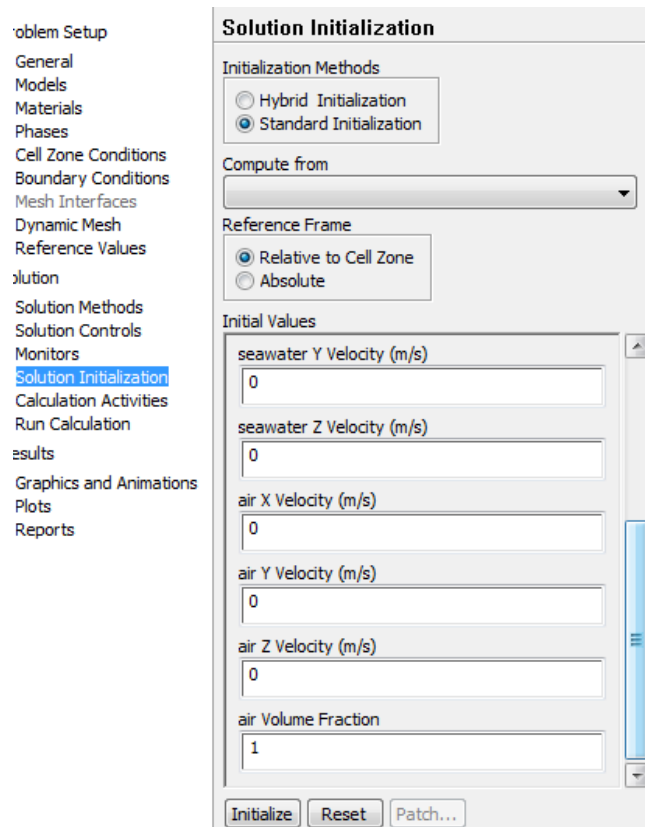


Figure D.11 Region adaption method

## Step 8: Solution initialization

Define → Solution initialization → initialize



Click Patch → Select air phase → Define volume fraction

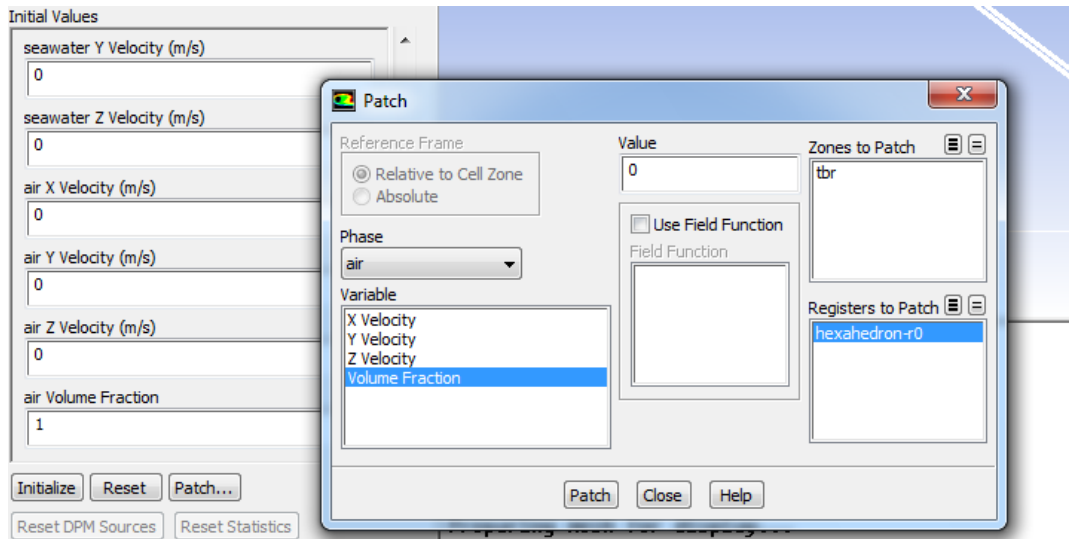


**Figure D.12** Solution initialization method

## **CURRICULUM VITAE**

**NAME** Miss Pinyaporn Wongluang

**DATE OF BIRTH** 16 June 1988

### **EDUCATIONAL RECORD**

**HIGH SCHOOL** High School Graduation  
Saipanya School under The Royal Patronage of Her Majesty The Queen, 2003

**BACHELOR'S DEGREE** Bachelor of Engineering (Chemical Engineering)  
Chulalongkorn University, 2009

**MASTER'S DEGREE** Master of Engineering (Chemical Engineering)  
King Mongkut's University of Technology Thonburi,  
2011